Nonlinear Control of a Quad Tilt-Wing UAV

by

Serhat Dikyar

Submitted to the Graduate School of Sabancı University
in partial fulfillment of the requirements for the degree of
Master of Science

Sabancı University

August 2011

Nonlinear Control of a Quad Tilt-Wing UAV

APPROVED BY:

Assoc. Prof. Dr. Mustafa Ünel
(Thesis Advisor)   ....

Prof. Dr. Asif Sabanovic   ....

Assoc. Prof. Dr. Kemalettin Erbatur   ....

Assoc. Prof. Dr. Kürşat Şendur   ....

Assist. Prof. Dr. Hakan Erdoğan   ....

DATE OF APPROVAL: 03/08/2011

Nonlinear Control of a Quad Tilt-Wing UAV

Serhat Dikyar

ME, Master's Thesis, 2011

Thesis Supervisor: Assoc. Prof. Mustafa Ünel

Keywords: UAV, Tilt-Wing, Quadrotor, Nonlinear Control, Dynamic
Inversion, Sliding Mode Control, Feedback Linearization

Abstract

Unmanned aerial vehicles (UAVs) have become increasingly more popular
over the last few decades. Their fascinating capabilities and performance
in accomplishing a specific task have made them indispensable for various
civilian/commercial and military applications. The remarkable progress in
advanced manufacturing techniques and electronic components have rendered
development of small, intelligent and low-cost UAVs possible. Consequently,
a significant amount of research effort has been devoted to design of UAVs
with intelligent navigation and control systems.

This thesis work focuses on nonlinear control of a quad tilt-wing un-
manned aerial vehicle (SUAVI: Sabanci University Unmanned Aerial Vehi-
cle). The aerial vehicle has the capability of vertical takeoff and landing
(VTOL), and flying horizontally due to its tilt-wing mechanism. Nonlin-
ear dynamical models for various flight modes are obtained. A hierarchical
control system that includes vertical, transition and horizontal modes flight
controllers is developed. In order to design these controllers, the dynamics of
the aerial vehicle is divided into position and attitude subsystems. Several
nonlinear position control methods are developed for different flight modes.
For the vertical flight mode, integral sliding mode and PID based position
controllers via dynamic inversion method are designed. Feedback lineariza-
tion and integral sliding mode attitude controllers are also proposed for the
attitude stabilization of the aerial vehicle in vertical, transition and horizon-
tal flight modes. Simulations and several real flight experiments demonstrate
success of the developed flight controllers.

Döner-Kanat Mekanizmalı bir İnsansız Hava Aracının Doğrusal Olmayan Kontrolü

Serhat Dikyar

ME, Master Tezi, 2011

Tez Danışmanı: Doç. Dr. Mustafa Ünel

Anahtar Kelimeler: İHA, Döner-Kanat, Dört-Rotor, Doğrusal Olmayan Kontrol, Dinamik Evirme, Kayan Kipli Kontrol, Geri Besleme ile Doğrusallaştırma

Özet

Son yıllarda İnsansız Hava Araçları (İHA) giderek daha yaygınlaşmaya başlamıştır. İHA'ların etkileyici kabiliyetleri ve verilen görevi tamamlamadaki başarıları, bu hava araçlarını birçok sivil ve askeri uygulamada vazgeçilmez hale getirmiştir. İleri üretim teknikleri ve elektronik ekipmanlardaki dikkat çekici gelişmeler küçük boyutlu, akıllı ve düşük maliyetli İHA'ların yapımını mümkün kılmıştır. Sonuç olarak, önemli derecede araştırma çabası akıllı navigasyon ve kontrol sistemlerine sahip İHA'ların tasarımına adanmıştır.

Bu tez çalışması döner kanat mekanizmasına sahip bir insansız hava aracı olan SUAVI'nin (Sabancı University Unmanned Aerial Vehicle) doğrusal olmayan kontrolüne odaklanmaktadır. Bu hava aracı döner-kanat mekanizması sayesinde dikine iniş-kalkış ve yatay uçuş özelliklerine sahiptir. Aracın değişik uçuş modları için doğrusal olmayan dinamik modeller elde edilmiş; dikey, geçiş ve yatay mod uçuş kontrolörlerini içeren bir hiyerarşik kontrol sistemi geliştirilmiştir. Bu kontrolörleri tasarlamak için araç dinamiği pozisyon ve yönelim olmak üzere iki alt sisteme ayrılmıştır. Hava aracının her üç uçuş modu için çeşitli doğrusal olmayan pozisyon kontrol yaklaşımları geliştirilmiştir. Aracın dikey uçuş modu için integral kayan kipli ve PID tabanlı pozisyon kontrol algoritmaları dinamik evirme methodu ile tasarlanmıştır. Bunun yanı sıra geri besleme ile doğrusallaştırma ve integral kayan kipli yönelim kontrolörleri aracın dikey, geçiş ve yatay uçuş modlarında yönelim stabilizasyonu için önerilmiştir. Geliştirilen kontrol yaklaşımlarının başarısı benzetim ve deney sonuçları ile doğrulanmıştır.

Acknowledgements

I would like to express my sincere gratitude and appreciation to my thesis advisor Assoc. Prof. Dr. Mustafa Ünel for his invaluable guidance, support, personal encouragements and bright insights throughout my M.S. study. I am greatly indebted to him for giving me the chance to carry out my M.S. thesis work in a motivating project environment.

I would like to thank Prof. Dr. Asif Sabanovic, Assoc. Prof. Dr. Kemalettin Erbatur, Assoc. Prof. Dr. Kürşat Şendur and Assist. Prof. Dr. Hakan Erdoğan for their feedbacks and spending their valuable time to serve as my jurors.

I would like to acknowledge the financial support provided by The Scientific & Technological Research Council of Turkey (TÜBİTAK) through BIDEB scholarship.

I would sincerely like to thank SUAVI project team members Ertuğrul Çetinsoy, Efe Sırımoğlu, Kaan Taha Öner and Cevdet Hançer for their pleasant team-work and efforts in this project. I would also like to thank Duruhan Özçelik and Tuğba Leblebici for their support and team-work in my other research project.

I would like to thank all mechatronics laboratory members for their precious friendship and the great time that we spent together throughout my M.S. study.

Finally, I would like to thank my entire extended family for all their love, motivation and the support throughout my life. They have always been there for me to overcome all challenges in my life.

Contents

List of Figures

List of Tables

Chapter I

1 Introduction

The remarkable progress in technology has extended the scope of the robotics over the last few decades. A great deal of robots have become a part of the human life. Their fascinating capabilities and performance in accomplishing a specific task have made them indispensable for various industrial, civil and military applications. They have even begun to replace humans in many critical tasks. Especially, autonomous mobile robots have become more involved in such tasks due to their wide range of application areas and enormous maneuvering capabilities. Although many other robots are restricted to operate on the ground, autonomous mobile robots have capability to work on the ground, the water and in the air. Among these robots, unmanned aerial vehicles (UAVs) have attracted attention of academic and industrial communities.

An UAV is defined as "an aerial vehicle that uses aerodynamic forces to provide vehicle lift, does not carry a human operator, can fly autonomously or be piloted remotely, can be expendable or recoverable, and can carry a lethal or non-lethal payload" [1]. The term UAV is commonly used by aerospace and robotics communities, but terms such as Remotely Piloted Vehicle (RPV), Remotely Operated Aircraft (ROA) and Unmanned Vehicle Systems (UVS) are also used to refer vehicles that are flying with no per-

son onboard. UAVs are primarily employed to perform tasks that are risky, monotonous and unreasonably expensive to be performed by a human pilot [2, 3]. Since there is no pilot onboard during operation, UAVs do not require very heavy and expensive protection systems or large enough space to carry a pilot. This leads UAVs to have the advantages of the reduced weight and smaller drag forces due to the removal of the cockpit and additionally the capability to endure a large amount of g-forces caused by sudden maneuvers [4]. Therefore many critical tasks, that manned aerial vehicles cannot perform, can be achieved by smaller and more compact UAVs. Moreover the decrease in size of air vehicles brings out another main advantage of UAVs that is decrease in manufacturing and operating cost [5]. The developments of advanced manufacturing techniques and electronic components that are computationally more powerful, smaller and lighter renders building of small, intelligent and low-cost UAVs possible.

The first UAV in the history was built by Elmer Sperry, who is the inventor of gyroscopes, in 1912 [6]. The designed airplane was the Curtiss seaplane with an installed gyro stabilized Sperry autopilot. Technological advances made by Sperry commence the genesis of unmanned flight [7]. Until 1950s the researches on UAVs did not demonstrate significant progress. In late 1950s various development programs were initiated due to the Cold War and Vietnam War [8]. These programs led to several reconnaissance aerial vehicles, such as the Firebee [9] and Lightning Bug [10]. However the modern UAV era has begun in 1970s. Research on UAV for the civilian application has also started in these years. In 1970 NASA conducted PA-30 research program to control an aircraft remotely from the ground station [8]. The main progress in UAV technology become eminent with the advance of elec-

tronic sensors and powerful microcomputers in 1990s. Research on UAVs was directed to construct aerial vehicles that can fly at high-altitude and have capability of long endurance. In this sense, NASA developed a unique aircraft, Proteus, for the application of atmospheric sampling and Earth monitoring in 1998 [11]. On the military side, Predator, which is the most famous UAV for military applications, was built and used by the U.S. Army in the Gulf War in 1991 [12]. Successful flights and accomplished missions of these aerial vehicles have led UAV industry to grow more quickly. UAVs have become more efficient with the installment of GPS (Global Positioning Sensor) and advanced image acquisition tools. In 2000s the Heron (Mahatz), which is medium altitude long endurance UAV, was developed by Israel Aerospace Industries. The aerial vehicle was designed to carry out 52 hours of strategic reconnaissance and surveillance missions at 35,000 feet [13]. Additionally, in 2009 the first autonomous ship landing was achieved by the RQ-8A Fire Scout that is vertical take-off and landing tactical unmanned air vehicle [14]. The evolution of the modern UAVs is depicted in Fig. 1.1 [15].

The application areas of UAVs is commonly divided into two categories which are civil and military. Today the civilian use, also referred as commercial use, of UAVs are far behind the military use. The total market revenue of the military applications is twenty eight times larger than the civilian market revenue [4]. However the growth rate of civilian/commercial market have begun to dominate military market that is worth billions of dollars. In the next ten to twenty years the civilian market for UAVs is expected to grow at a rate of four to five times faster than the military market. For the civilian use, many government agencies and private sector agencies are the potential users of UAV [16].
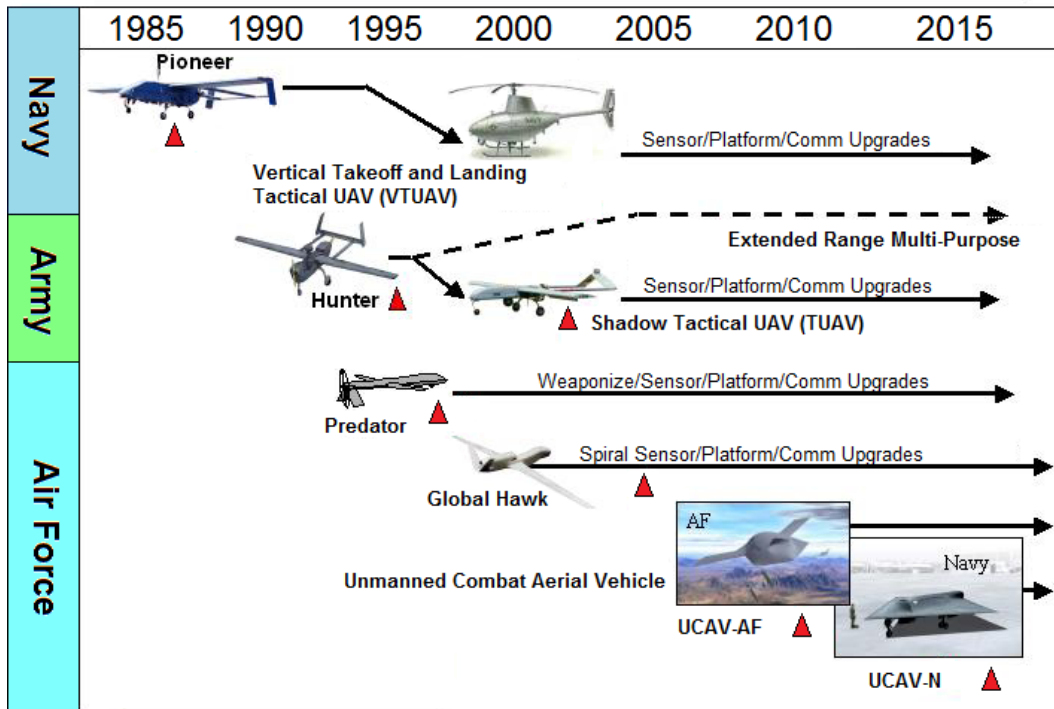
Figure 1.1: Evolution of Unmanned Aerial Vehicles [15]

Among many other civil/commercial applications, the most significants are listed below [16]:

- Communication Relay (equivalent to low-altitude satellites or cell towers)

- Media (overhead cameras for news and special events)

- Surveying (city and suburban planning)

- Farming and Ranching (check on cattle, fence lines, and work crews, spraying crops with pesticide and fertilizer, monitoring crops, soil, moisture, and pest conditions, and insect sampling)

- Customs & Border Protection (border patrols, surveys and control, counter narcotics and illegal alien surveillance)

4

- Film Industry (aerial photography and special effects)

- Archaeology (aerial observation of sites and digs)

- Oil and Mineral Industry (gas and oil pipeline monitoring in desolate areas, search for mineral and fossil fuel deposits)

- Energy Facilities (monitoring nuclear facilities, reconnaissance for hazardous waste cleanup, atmospheric and climatic research)

In addition to these civilian applications, UAVs are utilized in many military missions to reduce risks, workloads and direct enemy contact. The most critical military applications of UAVs can be listed as [17]:

- Reconnaissance and Surveillance (wide-area search and multi-intelligence capability, ability of processing, exploitation and dissemination)

- Security (operations to preserve friendly force combat power and freedom of maneuver)

- Close Combat (operating as a part of the combined arms team when conducting decisive, integrated, air-ground operations)

- Chemical, Biological, Radiological, Nuclear and High Yield Explosives Reconnaissance (The ability to find harmful material or hazards and to survey the affected areas)

- Interdiction Attack (degrading, neutralizing, or destroying enemy combat)

- Strike (conduct high risk and high payoff attack/strike operations with minimal exposure of manned systems)

- Target Identification and Designation (identify and precisely locate military targets in real-time)

- Combat Support (distinguish between friend, enemy, neutral, and non-combatant)

- Sustainment (supply/retrograde operations, extraction of damaged parts for repair)

Wide range of application areas of UAVs have resulted in various UAV types with different sizes, endurance levels and capabilities. Several different classifications have been proposed by international UAV communities. One of the major classifications based on flight altitude, endurance, speed and size is suggested by The European Association of Unmanned Vehicle Systems (EUROUVS) [18]. According to this classification, UAVs are mainly divided into three categories, namely Micro/Mini UAVs (MAVs/Mini), Tactical UAVs (TUAVs) and Strategic UAVs.

MAVs/Mini consists of the smallest UAVs that are under 30 kilograms and flying between 10-300 meters altitude with a maximum endurance of two hours. These aerial vehicles are suitable for urban and indoor flights as well as civil/commercial applications. EMT's FanCopter [19] and AeroVironment's Raven [20] falls into this category. Unlike MAVs/Mini, TUAVs, which are heavier aerial vehicles flying between 3000-8000 meters, are mostly designed to support military missions. The maximum take-off weight of these UAVs are range from 150 kilograms to 1500 kilograms, while their endurance limits vary between 2 to 48 hours. TUAVs are also divided into subcategories such as Close Range (CR), Short Range (SR), Long Range (LR) and Medium Altitude Long Endurance (MALE). Some of the TUAV examples are Elbit System's Hermes 1500 [21] and DRS Techologies' RQ-15 Neptune [22]. The last category is the Strategic UAVs that have capacity 12.000 kilograms maximum take-off weight and 20000 meters maximum flight altitude. This type of UAVs allows to accomplish various attractive civil tasks such as Earth observations as well as many critical military missions like interdiction attacks. Due to their ability to fly for long time and at high altitude, they are also called as HALE (High Altitude Long Endurance) UAVs. Some examples of

HALE UAVs are Northrop Grumman's RQ-4 Global Hawk [23] and NASA's Helios [24]. The aforementioned UAVs are tabulated in Table 1.1.

Table 1.1: Examples of different types of UAVs according to EUROUVS

Type of UAV	Institute/Company Name	Name of UAV	
Mini	EMT	FanCopter	
MAV	AeroVironmet	Raven	
Long Range	Elbit System	Hermes 1500	
MALE	DRS Techologies	RQ-15 Neptune	
HALE	Northrop Grumman	RQ-4 Global Hawk	
HALE	NASA	Helios	

UAVs can also be categorized by their mechanical structures and configurations such as fixed-wing, rotary-wing and hybrid designs [25]. The oldest researches on UAVs conducted on fixed-wing mechanism that generally refers to unmanned airplanes with wings. The advantage of fixed-wing UAVs stems from their capability of long endurance and high cruising speeds.

7

These aerial vehicles are also relatively simple to control [26]. Due to their high flight speed requirement, fixed-wing UAVs are not suitable for indoors and urban areas [27]. Similarly, requirement of runaway, launcher, net recovery or parachutes for takeoff and landing can be regarded as their significant disadvantages [28].

On the other hand, Rotary-wing UAVs, also called as rotorcraft or vertical takeoff and landing (VTOL) UAVs, do not necessitate any forward speed or runaway to initiate the flight. They are capable of high maneuverability and hovering. However, the significant drawbacks such as low flight speed and short endurance also exist for this type of UAVs. Among Rotary-wing UAVs, multiple rotor helicopters like quadrotors have attracted attention of increasing number of academic and industrial communities due to their relatively simple control architectures. The advantage of having fixed-pitch propellers instead of mechanically complex swashplate and transmission structures, and proportional thrust generation through propellers' rotational speeds ease both mechanical and control architecture of quadrotors [29].

Besides this conventional aerial vehicle designs, hybrid designs that combine advantages of fixed-wing and rotary-wing UAVs are becoming an increasing trend in UAV research area. The purpose of hybrid UAV designs is to integrate high speed and long range flight features of fixed-wing vehicles and vertical takeoff, landing and flight features of rotary-wing vehicles into one UAV design [30]. These hybrid vehicles can be classified as Tilt-Wing and Tilt-Rotor UAVs according to their mechanical structures. Tilt-Wing vehicles are capable of rotating its wings together with the rotor, whereas Tilt rotors can only rotate its propellers or rotors. This provides Tilt-Wing mechanisms to have significant advantage that is benefiting from aerody-

namic lift forces during horizontal flight [31]. Some of the examples of this categorization is given in Table 1.2.

Table 1.2: Examples of different types of UAVs according to their configurations

Type of UAV	Institute/Company Name	Name of UAV	
Fixed-Wing	AAI	Aerosonde [32]	
Fixed-Wing	Boeing	X-45B [33]	
Rotary-Wing	Draganfly Innovations	DraganFlyer X4 [34]	
Rotary-Wing	Microdrones	MD4-1000 [35]	
Tilt-Wing	Chiba University & G.H. Craft	QTW UAS-FS4 [36]	
Tilt-Rotor	Bell Company	Eagle Eye [37]	

The research on these various types of UAVs has mostly concentrated on control system, mechanical and aerodynamic design. Among these disciplines, control system is the indispensable part of the design procedure, since the design of control system is a crucial step to achieve basic tasks such as

9

reaching a desired location or precise trajectory tracking. The fundamental difficulties of control design arise from nonlinearities and couplings exist in the aerial vehicle dynamics. In order to cope with these difficulties, accurate dynamic modeling and investigation of these models are required. Since first design of UAVs, the researches have focused on aerial vehicle dynamics and developed numerous control algorithms to improve stability and maneuverability of the aerial vehicles in various flight conditions.

In literature many well-known linear control techniques are applied on various types of UAVs. In the work of Bouabdallah [38] et al. two model-based control techniques are implemented on an autonomous UAV called OS4. They proposed a classical PID technique that utilizes simplified dynamics and LQ based control approach based on a more complete model for the stabilization of OS4. Pounds et al. [39] developed a large quadrotor platform and analyzed flyer attitude dynamics to achieve best control sensitivity and disturbance rejection. They designed SISO linear controllers to stabilize the dominant decoupled pitch and roll modes. Mokhtari and Benallegue [40] proposed another linear control technique via state parameter control that is based on Euler angles and open loop positions state observer. A dynamic feedback controller was embedded to control structure to transform the closed loop part of the system into linear, controllable and decoupled dynamics. In [41], a LQ Servo controller augmented with a Kalman filter state observer was designed. In order to design the controller, the nonlinear model of quadrotor UAV was reduced to a controllable and observable linear model. Tayebi and McGilvray [42] presented quaternion-based PD feedback control scheme without compensation of the Coriolis and gyroscopic terms. Unlike the classical PD control structure, the proportional control was computed in

terms of the vector-quaternion and the derivative control was computed in terms of the airframe angular velocity.

Besides linear control techniques exist in the literature, nonlinear control approaches such as backstepping [43–46] and sliding mode control [47–51] are also proposed by many research groups due to their robustness against the external disturbances and model uncertainties. In the work of Madani and Benallegue [43] backstepping control was proposed to stabilize a rotary-wing UAV. The proposed method is based on backstepping control of the three interconnected subsystems. These subsystems are presented as the under-actuated subsystem that gives the relation of the horizontal positions with the pitch and roll angles, the fully-actuated subsystem that consists of the dynamics of the altitude and the heading, and the actuator subsystem that covers the dynamics of the propeller forces. Das et al. [44] introduced another backstepping control approach for a quadrotor helicopter. Unlike the other approaches that utilize state space form of aerial vehicle dynamics, the backstepping technique is applied on the Lagrangian form of the dynamics together with the two neural nets which are used for estimating the aerodynamic forces and moments.

In addition to pure backstepping approaches, sliding mode controllers and observers are also proposed with backstepping controllers. The work presented in [47, 48] introduced the design of a backstepping controller using sliding mode estimation technique. The difference of this approach from the typical backstepping is that the virtual control inputs are designed in terms of the previous time-step virtual control input estimations that are based on the exact second-order sliding mode differentiator. Besnard et al. [49] presented a robust multiple-loop and multiple time-scale flight controller based

on sliding mode disturbance observer approach that allows continuous control robust to external disturbance and model uncertainties. The proposed method is verified by simulations that demonstrate the robustness against external disturbances including wind, collision and actuator failure as well as model uncertainties.

Another commonly used control technique is feedback linearization [52–56] which is generally utilized with other control approaches. In [52, 53], a feedback linearization-based controller with a sliding mode observer is introduced. In addition to observer-controller structure, an adaptive estimator is also embedded to the the system to estimate external disturbances. The overall observer-estimator-control law is designed to regulate aerial vehicle with minimal number of sensors. Fang et al. [54] proposed a continuous sliding mode control method based on feedback linearization and an output tracking control. The continuous sliding mode control is achieved by dynamical extension of the nonlinear system and zero dynamics problem is handled by introducing two integrators in front of partial control input.

Alternatively robust neural networks [57–60] and H_∞ control [61–63] schemes are also proposed as the nonlinear control approaches. In the work of Dierks and Jagannathan [57, 58] neural networks and output feedback controllers that are based on learning the complete dynamics including uncertain nonlinear terms is presented. All six degrees of freedom of the UAV is controlled by a novel neural network virtual control input scheme and an output feedback control law is designed for the scenario in which only the position and the attitude information is available. Raffo et al. [61] introduced an integral predictive and nonlinear robust control strategy. In this hierarchical control scheme, a model predictive controller is employed for position

12

control and a nonlinear H_∞ controller is used for the stabilization of the rotational movement in the presence of aerodynamic disturbances, parametric and structural uncertainties.

1.1 Motivation

The recent developments in UAV design has become an exciting research area for mechatronics. Many research groups have been involved in various types of UAV design projects. Some of them have focused on fixed-wing UAVs like airplanes that have the advantage of long range flight with high speed capabilities, whereas some research groups have interested in rotary wings like helicopters that have the advantage of VTOL with the capability of high maneuverability. Besides this conventional aerial vehicle designs, hybrid designs that combine advantages of fixed-wing and rotary-wing UAVs have attracted attention of rapidly increasing number of research groups.

One of the most preferred hybrid design in academia is the Tilt-Wing mechanisms. As other hybrid designs, Tilt-Wing UAVs do not suffer from the requirement of runaways or special launching systems for takeoff and landing as well as the short flight ranges and the low flight speeds. These Tilt-Wing designs demonstrate the hover performance and control features of a helicopter together with the cruise speed and efficiency of an airplane. They are also superior than Tilt Rotor UAVs since the air flow produced by the rotors is blocked at a minimum level in tilt-wing structure.

Among Tilt-Wing configurations, Quad Tilt-Wing UAVs have been the subject of an increasing research interest during the last decade. Quad Tilt-Wing design, that consists of tandem tilt-wings and four rotors mounted on midspan of each wing, has the advantage of being a quadrotor which does not

13

necessitate any cyclic control, and the advantage of being an airplane that has efficient energy consumption features during long range flights. This advantage of combining the quadrotor and the airplane in the same mechanism brings out a new challenge that is the necessity of different flight modes and control structures based on the requirements of the present flight and the wing angles. Since the characteristics and the response of the Quad Tilt-Wing UAVs vary in accordance with flight modes, different flight controllers must be design to achieve stable and safe flight for all flight modes. Besides, nonlinear and robust control structures are required to cope with the model uncertainties and the external disturbances.

1.2 Thesis Organization and Contributions

In Chapter II, a full nonlinear dynamical model including explicit mathematical models for various flight modes and attitude dynamics expressed in world frame without hover assumption is obtained using Newton-Euler method.

Chapter III explains the hierarchical control architecture together with flight control system design and electronic control hardware. Several position control approaches proposed for vertical, transition and horizontal flight modes of the aerial vehicle. For the vertical flight mode, integral sliding mode and PID based position controllers via dynamic inversion method are introduced. Feedback linearization and integral sliding mode attitude controllers are also proposed for the attitude stabilization of the aerial vehicle in all three flight modes.

Chapter IV focuses on the simulations and experimental results of the proposed control architecture. Simulation results that compare integral sliding

mode position and attitude controllers with PID based position and feedback linearization attitude controllers are presented for the vertical mode of the aerial vehicle. A full flight scenario simulation that covers all three flight modes of the aerial vehicle is also provided to verify various flight mode controllers. Finally, the experimental results from the real flight test is presented to demonstrate performance of the proposed controllers.

Chapter V concludes the thesis work and indicates possible future directions.

Contributions of the thesis can be summarized as follows:

- A full nonlinear dynamical model including explicit mathematical models for various flight modes and attitude dynamics expressed in world frame without hover assumption is derived using Newton-Euler method.

- Flight controllers, which cover position and attitude controllers, are designed for vertical, transition and horizontal flight modes of the aerial vehicle.

- Integral sliding mode and PID based position controllers via dynamic inversion method are proposed for vertical flight mode of SUAVI. Although there are some dynamic inversion methods exist in the literature for quadrotors, dynamic inversion method that depends on wing angles are not studied for tilt-wing or tilt-rotor quadrotors. The developments presented in this thesis provide new results for quadrotors that have tilted wings or rotors.

- Feedback linearization and integral sliding mode attitude controllers are designed and employed for all three flight modes of the aerial vehicle.

- Simulation results that compare performance of the proposed flight controllers for the vertical flight mode and a full flight simulation that includes various flight modes of the aerial vehicle are presented.

- Performance of proposed flight control system is verified by real flight experiments. Vertical and horizontal flights together with transition flight mode are successfully realized.

1.3 Notes

This Master Thesis work is carried out in the context of the TÜBİTAK (The Scientific & Technological Research Council of Turkey) project "Mechanical Design, Prototyping and Flight Control of an Unmanned Autonomous Aerial Vehicle" under the grant number 107M179.

Produced journal and conference papers are:

- Design and Construction of a Novel Quad Tilt-Wing UAV, E. Çetinsoy, **S. Dikyar**, K. T. Öner, E. Sırımoğlu, C. Hancçer, M. Ünel, M. F. Akşit, Elsevier Journal of Mechatronics, 2011. (under review)

- Flight Controller Design for Vertical, Transition and Horizontal Modes of a Tilt-Wing Quadrotor, **S. Dikyar**, E. Çetinsoy, M. Ünel, IEEE International Conference on Automation, Robotics and Applications (ICARA 2011), December 6-8. (submitted)

- Döner Kanatlı Quadrotor için Dikey, Geçiş ve Yatay Modları Uçuş Denetleyicileri Tasarımı, **S. Dikyar**, E. Çetinsoy, M. Ünel, TOK'11: Otomatik Kontrol Ulusal Toplantısı, September 14-16.

1.4 Nomenclature

Symbol	Description
A	area of the wing
$\mathbb{B}$	inverse of rotational velocity transformation matrix
c_D	drag coefficient
c_L	lift coefficient
$C(\zeta)$	Coriolis matrix
$\mathbb{C}$	Coriolis matrix in inertial frame
$D(\zeta, \xi)$	external disturbance vector
e_{at}	orientation error vector for integral sliding mode attitude controllers
e_{ps}	position error vector for integral sliding mode position controllers
e_x	position error of the aerial vehicle along x axis
e_y	position error of the aerial vehicle along y axis
e_z	position error of the aerial vehicle along z axis
e_θ	orientation error of the aerial vehicle around y axis
e_ϕ	orientation error of the aerial vehicle around x axis
e_ψ	orientation error of the aerial vehicle around z axis
$E(\xi)w^2$	system actuator vector
$\mathbb{E}$	rotational velocity transformation matrix
F_d	forces due to external disturbances
F_D	drag forces
F_g	gravity force
F_L	lift forces
F_t	total external force acting on the aerial vehicle
F_{th}	thrust force created by rotors
F_w	aerodynamic forces generated by the wings
G	gravity vector
$\mathbb{G}$	mass matrix for integral sliding mode position controllers
$\widehat{\mathbb{G}}$	nominal value of $\mathbb{G}$ matrix
$\widetilde{\mathbb{G}}$	parameter error of $\mathbb{G}$ matrix
$\mathbb{H}$	new vector that includes disturbances, gravity and aerodynamic forces

Symbol	Description
$\widehat{\mathbb{H}}$	nominal value of $\mathbb{H}$ vector
$\widetilde{\mathbb{H}}$	parameter error of $\mathbb{H}$ vector
I_b	inertia matrix of the aerial vehicle in body fixed frame
I_{xx}	moment of inertia around x_b in body frame
I_{yy}	moment of inertia around y_b in body frame
I_{zz}	moment of inertia around z_b in body frame
J	Jacobian transformation between generalized vectors
J_{prop}	inertia of the propellers about their rotation axis
K_1	integral sliding mode position controller gain matrix for continuous part
K_2	integral sliding mode position controller gain for discontinuous part
K_3	integral sliding mode attitude controller gain matrix for continuous part
K_4	integral sliding mode attitude controller gain for discontinuous part
K_{dat}	derivative gain matrix for integral sliding mode attitude controllers
K_{pat}	proportional gain matrix for integral sliding mode attitude controllers
K_{dps}	derivative gain matrix for integral sliding mode position controllers
K_{pps}	proportional gain matrix for integral sliding mode position controllers
K_{dx}	derivative gain for PID based position controllers along x axis
K_{ix}	integral gain for PID based position controllers along x axis
K_{px}	proportional gain for PID based position controllers along x axis
K_{dy}	derivative gain for PID based position controllers along y axis
K_{iy}	integral gain for PID based position controllers along y axis
K_{py}	proportional gain for PID based position controllers along y axis
K_{dz}	derivative gain for PID based position controllers along z axis
K_{iz}	integral gain for PID based position controllers along z axis
K_{pz}	proportional gain for PID based position controllers along z axis
$K_{d\theta}$	derivative gain for controller around y axis
$K_{i\theta}$	integral gain for controller around y axis
$K_{p\theta}$	proportional gain for controller around y axis
$K_{d\phi}$	derivative gain for controller around x axis
$K_{i\phi}$	integral gain for controller around x axis
$K_{p\phi}$	proportional gain for controller around x axis

Symbol	Description
$K_{d\psi}$	derivative gain for controller around z axis
$K_{i\psi}$	integral gain for controller around z axis
$K_{p\psi}$	proportional gain for controller around z axis
l_l	rotor distance to center of gravity along x_b in body frame
l_s	rotor distance to center of gravity along y_b in body frame
m	mass of the aerial vehicle
M	inertia matrix
M_d	torques due to external disturbances
M_{gyro}	gyroscopic momoents
M_t	total moments acting on the aerial vehicle
M_{th}	rotor moments
M_w	aerodynamic moment due to lift/drag forces
$\mathbb{M}$	transformed inertia matrix of the aerial vehicle
$\widehat{\mathbb{M}}$	nominal value of $\mathbb{M}$ matrix
$\widetilde{\mathbb{M}}$	parameter error of $\mathbb{M}$ matrix
$\mathbb{N}$	new vector that contains Coriolis terms, gyroscopic effects, aerodynamic moments
$\widehat{\mathbb{N}}$	nominal value of $\mathbb{N}$ vector
$\widetilde{\mathbb{N}}$	parameter error of $\mathbb{N}$ vector
O_b	origin of body fixed frame
O_w	origin of inertial (world) frame
$O(\zeta)w$	gyroscopic matrix
p	angular velocity of the aerial vehicle along x_b in body frame
P	horizontal component of the total thrust
P_w	position of the aerial vehicle in inertial (world) frame
q	angular velocity of the aerial vehicle along y_b in body frame
Q	vertical component of the total thrust
r	angular velocity of the aerial vehicle along z_b in body frame
R_{wb}	orientation of body frame wrt. the world frame
R_{bw}	orientation of world frame wrt. the earth frame
s	sliding surface of integral sliding mode attitude controllers
s_0	linear combination of errors for integral sliding mode attitude controllers

Symbol	Description
v_x	linear velocity along x_b in body fixed frame
v_y	linear velocity along y_b in body fixed frame
v_z	linear velocity along z_b in body fixed frame
v_α	airstream velocity
V_1	Lyapunov function candidate for integral sliding mode position controllers
V_2	Lyapunov function candidate for integral sliding mode attitude controllers
V_w	linear velocity of the aerial vehicle in inertial (world) frame
V_b	linear velocity of the aerial vehicle in body fixed frame
W_t	aerodynamic forces around y axis
W_x	aerodynamic forces along x axis
W_y	aerodynamic forces along y axis
W_z	aerodynamic forces along z axis
x_b	x axis of body fixed frame
x_w	x axis of inertial (world) frame
X	position of the aerial vehicle along x_w in inertial frame
X_d	desired position of the aerial vehicle along x_w in inertial frame
y_b	y axis of body fixed frame
y_w	y axis of inertial frame
Y	position of the aerial vehicle along y_w in inertial frame
Y_d	desired position of the aerial vehicle along y_w in inertial frame
z_b	z axis of body fixed frame
z_{at}	integral term for integral sliding mode attitude controllers
z_{ps}	integral term for integral sliding mode position controllers
z_w	z axis of inertial (world) frame
Z	position of the aerial vehicle along z_w in inertial (world) frame
Z_d	desired position of the aerial vehicle along z_w in inertial frame
α_w	attitude of the aerial vehicle in inertial frame
α_i	effective angle of attack
γ_1	auxiliary variable for PID based vertical mode position controllers
γ_2	auxiliary variable for PID based vertical mode position controllers
γ_3	auxiliary variable for integral SMC vertical mode position controllers

Symbol	Description
γ_4	auxiliary variable for integral SMC vertical mode position controllers
Γ_1	new parameter error vector for integral sliding mode position controllers
Γ_2	new parameter error vector for integral sliding mode position controllers
Γ_3	new parameter error vector for integral sliding mode attitude controllers
Γ_4	new parameter error vector for integral sliding mode attitude controllers
ω_i	propellers rotational speed
Ω_b	angular velocity of the aerial vehicle in body fixed frame
θ	pitch angle, angular position around y_w
θ_d	desired pitch angle
ϕ	roll angle, angular position around x_w
ϕ_d	desired roll angle
ψ	yaw angle, angular position around z_w
ψ_d	desired yaw angle
θ_i	angle of attack for each wing
ρ	air density
σ	sliding surface of integral sliding mode position controllers
σ_0	linear combination of errors for integral sliding mode position controllers
λ_i	torque/force ratio
μ_1	virtual control input for x axis
μ_2	virtual control input for y axis
μ_3	virtual control input for z axis
$\tilde{\mu_1}$	new virtual control input for x axis
$\tilde{\mu_2}$	new virtual control input for y axis
$\tilde{\mu_3}$	new virtual control input for z axis
ζ	generalized velocity vector of the aerial vehicle
ξ	position and orientation of the aerial vehicle in inertial (world) frame
η	virtual control input vector for feedback linearization attitude controllers
η_1	virtual control input around x for feedback linearization attitude controllers
η_2	virtual control input around y for feedback linearization attitude controllers
η_3	virtual control input around z for feedback linearization attitude controllers
$\tilde{\eta}$	new virtual control input vector for feedback linearization attitude controllers

Symbol	Description
$\tilde{\eta}_1$	new virtual control input around x for feedback linearization attitude controllers
$\tilde{\eta}_2$	new virtual control input around y for feedback linearization attitude controllers
$\tilde{\eta}_3$	new virtual control input around z for feedback linearization attitude controllers
τ	integral sliding mode attitude control input vector
$\widehat{\tau}$	continuous part of integral sliding mode attitude control input
$\bar{\tau}$	virtual control input vector for integral sliding mode attitude control
$\bar{\tau}_1$	virtual control input of integral sliding mode position control input for ϕ
$\bar{\tau}_2$	virtual control input of integral sliding mode position control input for θ
$\bar{\tau}_3$	virtual control input of integral sliding mode position control input for ψ
τ_s	discontinuous part of integral sliding mode attitude control input
τ_{seq}	equivalent control of integral sliding mode attitude control input
F	integral sliding mode position control input vector
$\widehat{F}$	continuous part of integral sliding mode position control input
F_1	integral sliding mode position control input for x axis
F_2	integral sliding mode position control input for y axis
F_3	integral sliding mode position control input for z axis
F_s	discontinuous part of integral sliding mode position control input
F_{seq}	equivalent control of integral sliding mode position control input

Chapter II

2 Mathematical Model of SUAVI

The operational requirements of an air vehicle has a significant effect on the design procedure. SUAVI is aimed to operate in indoor-outdoor surveillance missions such as security patrolling, traffic control and disasters. It is designed as an electric powered Quad Tilt-Wing UAV in which four motors are placed on the mid-span leading-edges of wings. In this design, the wings can be tilted vertical-horizontal position range (Fig. 2.1).

(a)

(b)

Figure 2.1: Various flight modes of SUAVI

When the wings are in the vertical position, i.e. quadrotor configuration, lift forces are produced by motor thrusts for takeoff, landing and hover. On the other hand, when horizontal flight is required, wings are tilted gradually to the desired angles obtained from wind tunnel tests. The wings are tilted to nearly horizontal position, i.e. tandem wing airplane configuration, when high speed is needed. In this configuration, lift forces are generated by the wings and vertical components of the motor thrusts, whereas horizontal components produce forward thrust to obtain high speed. The design length and wingspan are 1 m, and the design weight is roughly 4.5 kg.

2.1 Mathematical Modeling

SUAVI has a complicated structure that can change flight modes in accordance with required flight speed. The dynamics of the system is affected from these flight modes significantly since the response of the aerial vehicle highly depends on the wing angle of attacks. Therefore a detailed mathematical model of the system has to be developed. In this section, the the full nonlinear mathematical model of SUAVI is derived and this model is investigated in various flight modes.

In deriving dynamical model of the aerial vehicle the following assumptions are made [64]:

- The aerial vehicle is a 6 DOF a rigid body.
- The center of mass and origin of body fixed frames are coincident.
- The drag force of the fuselage is neglected.
- The relative airspeed on the body frame is only due to vehicle's flight speed.

2.1.1 Kinematics of the Aerial Vehicle

Two reference frames are utilized in the mathematical modeling of the aerial vehicle. They are the World frame $W : (O_w, x_w, y_w, z_w)$ and the Body frame $B : (O_b, x_b, y_b, z_b)$. In the earth fixed inertial reference frame (world frame), x_w is directed northwards, y_w is directed eastwards, z_w is directed downwards and O_w is the origin of the world frame. Similarly, in the body frame, x_b is directed to the front of the vehicle, y_b is directed to the right of the vehicle, z_b is directed downwards and O_b is the origin at the center of mass of the aerial vehicle.

The position and linear velocity of the vehicle's center of mass in the world frame are expressed as

$$P_w = [X, Y, Z]^T, \quad V_w = \dot{P}_w = [\dot{X}, \dot{Y}, \dot{Z}]^T \tag{2.1}$$

Vehicle's attitude and its time derivative in the world frame are defined as

$$\alpha_w = [\phi, \theta, \psi]^T, \quad \Omega_w = \dot{\alpha}_w = [\dot{\phi}, \dot{\theta}, \dot{\psi}]^T \tag{2.2}$$

where ϕ, θ and ψ are roll, pitch and yaw angles, respectively. The orientation of the body frame with respect to the world frame is expressed by the rotation matrix

$$R_{wb}(\phi, \theta, \psi) = \begin{bmatrix} c_\psi c_\theta & s_\phi s_\theta c_\psi - c_\phi s_\psi & c_\phi s_\theta c_\psi + s_\phi s_\psi \\ s_\psi c_\theta & s_\phi s_\theta s_\psi + c_\phi c_\psi & c_\phi s_\theta s_\psi - s_\phi c_\psi \\ -s_\theta & s_\phi c_\theta & c_\phi c_\theta \end{bmatrix} \tag{2.3}$$

In this equation $c_{(.)}$ and $s_{(.)}$ denotes $\cos(.)$ and $\sin(.)$, respectively. The transformation of linear velocities between the world and the body frames is also given by this rotation matrix as

$$V_b = \begin{bmatrix} v_x \\ v_y \\ v_z \end{bmatrix} = R_{wb}^T(\phi, \theta, \psi) \cdot V_w = R_{bw}(\phi, \theta, \psi) \cdot V_w \tag{2.4}$$

The relation between the angular velocity of the vehicle and the time derivative of the attitude angles is given by the following transformation

$$\Omega_b = \begin{bmatrix} p \\ q \\ r \end{bmatrix} = \mathbb{E}(\alpha_w) \cdot \Omega_w = \mathbb{E}(\alpha_w) \cdot \begin{bmatrix} \dot{\phi} \\ \dot{\theta} \\ \dot{\psi} \end{bmatrix} \tag{2.5}$$

where $\mathbb{E}$ is the velocity transformation matrix and defined as (see Appendix A for the derivation)

$$\mathbb{E}(\alpha_w) = \begin{bmatrix} 1 & 0 & -s_\theta \\ 0 & c_\phi & s_\phi c_\theta \\ 0 & -s_\phi & c_\phi c_\theta \end{bmatrix} \tag{2.6}$$

Inverse of the velocity transformation is denoted as $\mathbb{B}(\alpha_w)$ and implies

$$\Omega_w = \mathbb{E}^{-1}(\alpha_w) \cdot \Omega_b = \mathbb{B}(\alpha_w) \cdot \Omega_b \tag{2.7}$$

2.1.2 Dynamics of the Aerial Vehicle

Assuming the aerial vehicle as a 6 DOF rigid body, the dynamical model of SUAVI can be derived by using Newton-Euler formulation. The position dynamics is expressed in world frame, whereas the attitude dynamics is expressed in body fixed frame. Hence the dynamics of the aerial vehicle can be written as

$$\begin{bmatrix} mI & 0 \\ 0 & I_b \end{bmatrix} \begin{bmatrix} \dot{V}_w \\ \dot{\Omega}_b \end{bmatrix} + \begin{bmatrix} 0 \\ \Omega_b \times (I_b \Omega_b) \end{bmatrix} = \begin{bmatrix} F_t \\ M_t \end{bmatrix} \quad\quad (2.8)$$

where the subscripts w and b express the vector and matrix quantities in world and body frames, respectively. m denotes the mass and I_b denotes the vehicle's inertia matrix. I and 0 are 3×3 identity and zero matrices, respectively. The right hand side of Eqn. (2.8) includes the total force F_t and total moment M_t. For a quad tilt-wing aerial vehicle, these forces and moments are functions of the motor thrusts, forces on the wings and the fuselage, and also the wing angle of attacks. These forces and moments are depicted in Figure 2.2.
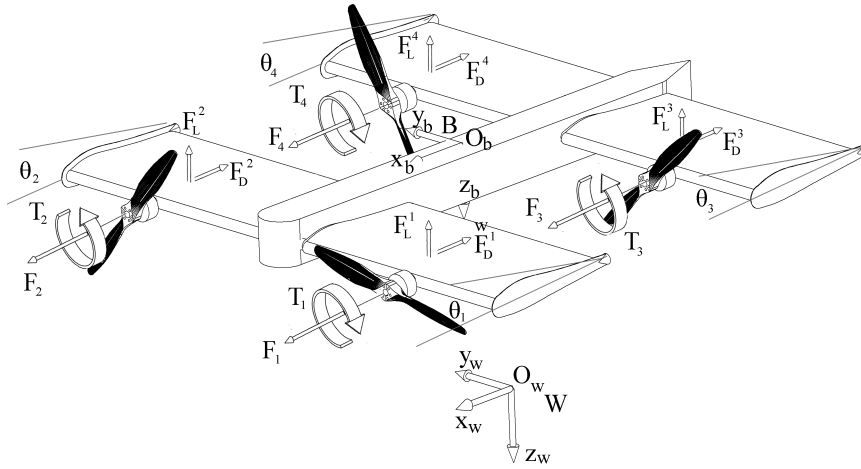

Figure 2.2: External forces and moments acting on the vehicle

The total external force acting on the system F_t consists of the motor thrusts F_{th}, aerodynamic forces on the wings F_w, gravity force on the vehicle F_g and external disturbances such as winds and gusts F_d. Since these forces

27

are expressed in the body frame, they have to be transformed by R_{wb} to be expressed in the world frame as follows

$$F_t = R_{wb}(F_{th} + F_w + F_g + F_d) \tag{2.9}$$

where these force vectors are derived as

$$F_{th} = \begin{bmatrix} c_{\theta_1} & c_{\theta_2} & c_{\theta_3} & c_{\theta_4} \\ 0 & 0 & 0 & 0 \\ -s_{\theta_1} & -s_{\theta_2} & -s_{\theta_3} & -s_{\theta_4} \end{bmatrix} \begin{bmatrix} k\omega_1{}^2 \\ k\omega_2{}^2 \\ k\omega_3{}^2 \\ k\omega_4{}^2 \end{bmatrix}$$

$$F_w = \begin{bmatrix} (F_D^1 + F_D^2 + F_D^3 + F_D^4) \\ 0 \\ (F_L^1 + F_L^2 + F_L^3 + F_L^4) \end{bmatrix}$$

and

$$F_g = \begin{bmatrix} -s_\theta \\ s_\phi c_\theta \\ c_\phi c_\theta \end{bmatrix} mg$$

In these equations, θ_i denotes wing angles with respect to the body. Note that the motor thrusts are modeled as

$$F_i = k\omega_i^2 \tag{2.10}$$

where ω_i is the rotor rotational speed.

To simplify the design of the aerial vehicle, left and right wings both at the back and at the front are tilted together, leading to the relations $\theta_1 = \theta_2$

and $\theta_3 = \theta_4$. The lift forces $F_L^i(\theta_i, v_x, v_z)$ and the drag forces $F_D^i(\theta_i, v_x, v_z)$ are functions of linear velocities v_x and v_z, and the wing angle of attacks θ_i, namely

$$
\begin{bmatrix} F_D^i \\ 0 \\ F_L^i \end{bmatrix} = R(\theta_i - \alpha_i) \begin{bmatrix} -\frac{1}{2} c_D(\alpha_i) \rho A v_\alpha^2 \\ 0 \\ -\frac{1}{2} c_L(\alpha_i) \rho A v_\alpha^2 \end{bmatrix} \tag{2.11}
$$

where

$$
v_\alpha = \sqrt{v_x^2 + v_z^2}
$$

$$
\alpha_i = \theta_i - (-atan2(v_z, v_x))
$$

In these equations, ρ is the air density, A is the wing planform area, v_α is the airflow velocity and α_i is the effective angle of attack of the wing with respect to the air flow as depicted in Figure 2.3. $R(\theta_i - \alpha_i)$ is the rotation matrix for the rotation around y axis that decomposes the forces on the wings onto the body axes.
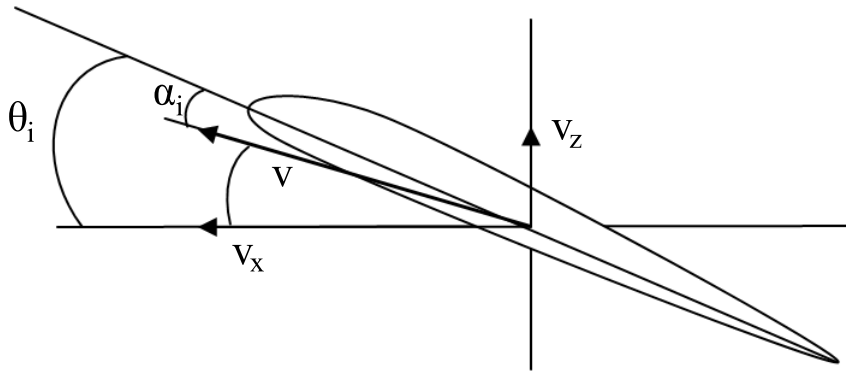

Figure 2.3: Effective angle of attack α_i

The total moment M_t consists of the moments generated by the rotors M_{th}, moments generated by the aerodynamic forces produced by the wings

M_w, moments generated by the gyroscopic effects of the propellers M_{gyro} and moments due to the external disturbances M_d; i.e.

$$M_t = M_{th} + M_w + M_{gyro} + M_d \qquad (2.12)$$

where

$$M_{th} = l_s \begin{bmatrix} s_{\theta_1} - \frac{\lambda_1}{l_s}c_{\theta_1} & -s_{\theta_2} - \frac{\lambda_2}{l_s}c_{\theta_2} & s_{\theta_3} - \frac{\lambda_3}{l_s}c_{\theta_3} & -s_{\theta_4} - \frac{\lambda_4}{l_s}c_{\theta_4} \\ \frac{l_l}{l_s}s_{\theta_1} & \frac{l_l}{l_s}s_{\theta_2} & -\frac{l_l}{l_s}s_{\theta_3} & -\frac{l_l}{l_s}s_{\theta_4} \\ c_{\theta_1} + \frac{\lambda_1}{l_s}s_{\theta_1} & -c_{\theta_2} + \frac{\lambda_2}{l_s}s_{\theta_2} & c_{\theta_3} + \frac{\lambda_3}{l_s}s_{\theta_3} & -c_{\theta_4} + \frac{\lambda_4}{l_s}s_{\theta_4} \end{bmatrix} \begin{bmatrix} k\omega_1{}^2 \\ k\omega_2{}^2 \\ k\omega_3{}^2 \\ k\omega_4{}^2 \end{bmatrix}$$

$$M_w = \begin{bmatrix} l_s(F_L^1 - F_L^2 + F_L^3 - F_L^4) \\ l_l(F_L^1 + F_L^2 - F_L^3 - F_L^4) \\ l_s(-F_D^1 + F_D^2 - F_D^3 + F_D^4) \end{bmatrix}$$

and

$$M_{gyro} = \sum_{i=1}^{4} J_{prop}[\eta_i \Omega_b \times \begin{bmatrix} c_{\theta_i} \\ 0 \\ -s_{\theta_i} \end{bmatrix} \omega_i]$$

In these expressions, l_s and l_l denote the spanwise and longitudinal distances between the rotors and the center of mass of the vehicle, respectively. J_{prop} is the rotational inertia of the rotors about their rotation axes and $\eta_{(1,2,3,4)} = 1, -1, -1, 1$. The rotor reaction torques are modeled as

$$T_i = \lambda_i k \omega_i^2 \qquad (2.13)$$

where λ_i are torque/force ratios. For clockwise rotating propellers, $\lambda_{2,3} = -\lambda$ whereas for counterclockwise rotating propellers $\lambda_{1,4} = \lambda$.

Note that the sum of moments generated by the rotors result in only a roll moment in vertical flight mode, whereas in transition and horizontal modes these moments result in yaw and roll moments. Similarly, the total thrust forces produced by rotors generate pure lift forces in vertical flight mode, whereas these forces cause roll moment and lift forces in transition and horizontal flight modes.

Utilizing vector-matrix notation and including external disturbances, the dynamics of SUAVI can be rewritten in a more compact form as

$$M\dot{\zeta} + C(\zeta)\zeta = G + O(\zeta)\omega + E(\xi)\omega^2 + W(\zeta) + D(\zeta, \xi) \tag{2.14}$$

where $\zeta = [\dot{X}, \dot{Y}, \dot{Z}, p, q, r]^T$ is the generalized velocity vector and $\xi = [X, Y, Z, \phi, \theta, \psi]^T$ is the position and the orientation (pose) of the vehicle expressed in the world frame. The relation between ζ and ξ is given by the following Jacobian transformation:

$$\dot{\xi} = J\zeta \Rightarrow \begin{bmatrix} \dot{X} \\ \dot{Y} \\ \dot{Z} \\ \dot{\phi} \\ \dot{\theta} \\ \dot{\psi} \end{bmatrix} = \begin{bmatrix} 1 & 0 & 0 & 0 & 0 & 0 \\ 0 & 1 & 0 & 0 & 0 & 0 \\ 0 & 0 & 1 & 0 & 0 & 0 \\ 0 & 0 & 0 & 1 & s_\phi t_\theta & c_\phi t_\theta \\ 0 & 0 & 0 & 0 & c_\phi & -s_\phi \\ 0 & 0 & 0 & 0 & s_\phi/c_\theta & c_\phi/c_\theta \end{bmatrix} \begin{bmatrix} \dot{X} \\ \dot{Y} \\ \dot{Z} \\ p \\ q \\ r \end{bmatrix} \tag{2.15}$$

Note that the bottom-right 3×3 submatrix of the Jacobian is the inverse of $\mathbb{E}$, i.e. the $\mathbb{B}$ matrix defined in Eqn. (2.7).

The mass-inertia matrix M, the Coriolis-centripetal matrix $C(\zeta)$, the gyroscopic term $O(\zeta)\omega$ and the gravity term G, are defined as

$$M = \begin{bmatrix} mI_{3x3} & 0_{3x3} \\ 0_{3x3} & diag(I_{xx}, I_{yy}, I_{zz}) \end{bmatrix} \tag{2.16}$$

$$C(\zeta) = \begin{bmatrix} 0 & 0 & 0 & 0 & 0 & 0 \\ 0 & 0 & 0 & 0 & 0 & 0 \\ 0 & 0 & 0 & 0 & 0 & 0 \\ 0 & 0 & 0 & 0 & I_{zz}r & -I_{yy}q \\ 0 & 0 & 0 & -I_{zz}r & 0 & I_{xx}p \\ 0 & 0 & 0 & I_{yy}q & -I_{xx}p & 0 \end{bmatrix} \tag{2.17}$$

$$O(\zeta)\omega = J_{prop} \begin{pmatrix} 0_{3 \times 1} \\ \sum_{i=1}^{4}[\eta_i\Omega_b \times \begin{bmatrix} c_{\theta_i} \\ 0 \\ -s_{\theta_i} \end{bmatrix} \omega_i] \end{pmatrix} \tag{2.18}$$

$$G = \begin{bmatrix} 0 & 0 & mg & 0 & 0 & 0 \end{bmatrix}^T \tag{2.19}$$

where I_{xx}, I_{yy} and I_{zz} are the moments of inertia of the aerial vehicle around its body frame axes. Lift and drag forces produced by the wings and the resulting moments due to these forces for different wing angles are defined as

$$W(\zeta) = [W_x, W_y, W_z, 0, W_t, 0]^T =$$

$$\begin{bmatrix} R_{wb} \begin{bmatrix} 2(F_D^f(\theta_f, v_x, v_z) + F_D^r(\theta_r, v_x, v_z)) \\ 0 \\ 2(F_L^f(\theta_f, v_x, v_z) + F_L^r(\theta_r, v_x, v_z)) \end{bmatrix} \\ 0 \\ 2l_l(F_L^f(\theta_f, v_x, v_z) - F_L^r(\theta_r, v_x, v_z)) \\ 0 \end{bmatrix} \qquad (2.20)$$

where $F_L^i(\theta_i, v_x, v_z)$ and $F_D^i(\theta_i, v_x, v_z)$ are the lift and drag forces produced at the wings and $i = f, r$ subscripts denote front and rear angles, respectively. W_x, W_y and W_z are aerodynamic forces along X, Y, Z axis of world coordinate frame and W_t is the moment produced by aerodynamic forces around Y axis of body fixed coordinate frame.

System actuator vector, $E(\xi)\omega^2$, is defined as

$$E(\xi)\omega^2 = \begin{bmatrix} R_{wb} F_{th} \\ M_{th} \end{bmatrix} = \begin{bmatrix} (c_\phi s_\theta c_\psi + s_\phi s_\psi)u_v + c_\psi c_\theta u_h \\ (c_\phi s_\theta s_\psi - s_\phi c_\psi)u_v + s_\psi c_\theta u_h \\ c_\phi c_\theta u_v - s_\theta u_h \\ (l_s s_{\theta_f} - \lambda c_{\theta_f})u_{f_{dif}} + (l_s s_{\theta_r} + \lambda c_{\theta_r})u_{r_{dif}} \\ [u_{f_{sum}} s_{\theta_f} - u_{r_{sum}} s_{\theta_r}]l_l \\ (l_s c_{\theta_f} + \lambda s_{\theta_f})u_{f_{dif}} + (l_s c_{\theta_r} - \lambda s_{\theta_r})u_{r_{dif}} \end{bmatrix} \qquad (2.21)$$

where

$$u_{f_{dif}} = k(\omega_1^2 - \omega_2^2), \quad u_{r_{dif}} = k(\omega_3^2 - \omega_4^2), \quad u_{f_{sum}} = k(\omega_1^2 + \omega_2^2),$$

$$u_{r_{sum}} = k(\omega_3^2 + \omega_4^2), \quad u_v = -s_{\theta_f} u_{f_{sum}} - s_{\theta_r} u_{r_{sum}},$$

$$u_h = c_{\theta_f} u_{f_{sum}} + c_{\theta_r} u_{r_{sum}}, \quad \theta_f = \theta_1 = \theta_2, \quad \theta_r = \theta_3 = \theta_4$$

To simplify the analysis, in the sequel the aerodynamic downwash effect of front wings on the rear wings will be neglected and the front and rear wing angles are assumed to be equal $(\theta_f = \theta_r)$. In this case the system actuator vector becomes

$$E(\xi)\omega^2 = \begin{bmatrix} (c_\psi c_\theta c_{\theta_f} - (c_\phi s_\theta c_\psi + s_\phi s_\psi)s_{\theta_f})u_1 \\ (s_\psi c_\theta c_{\theta_f} - (c_\phi s_\theta s_\psi - s_\phi c_\psi)s_{\theta_f})u_1 \\ (-s_\theta c_{\theta_f} - c_\phi c_\theta s_{\theta_f})u_1 \\ s_{\theta_f} u_2 - c_{\theta_f} u_4 \\ s_{\theta_f} u_3 \\ c_{\theta_f} u_2 + s_{\theta_f} u_4 \end{bmatrix} \tag{2.22}$$

Control inputs $u_{1,2,3,4}$ used in Eqn. (2.22) are explicitly written below:

$$u_1 = k(\omega_1^2 + \omega_2^2 + \omega_3^2 + \omega_4^2) \tag{2.23}$$

$$u_2 = kl_s(\omega_1^2 - \omega_2^2 + \omega_3^2 - \omega_4^2) \tag{2.24}$$

$$u_3 = kl_l(\omega_1^2 + \omega_2^2 - \omega_3^2 - \omega_4^2) \tag{2.25}$$

$$u_4 = k\lambda(\omega_1^2 - \omega_2^2 - \omega_3^2 + \omega_4^2) \tag{2.26}$$

Neglecting the wing forces and setting $\theta_f = \theta_r = \pi/2$, the dynamics of the aerial vehicle resembles a quadrotor model reported in the literature [43, 45]. Position and attitude dynamics of the aerial vehicle in quadrotor mode can be expressed as follows:

$$\ddot{X} = \frac{1}{m}(-c_\phi s_\theta c_\psi - s_\phi s_\psi)u_1$$

$$\ddot{Y} = \frac{1}{m}(-c_\phi s_\theta s_\psi + s_\phi c_\psi)u_1$$

$$\ddot{Z} = -\frac{c_\phi c_\theta}{m}u_1 + g$$

$$\dot{p} = \frac{u_2}{I_{xx}} + \frac{I_{yy} - I_{zz}}{I_{xx}}qr - \frac{J_{prop}}{I_{xx}}q\omega_p$$

$$\dot{q} = \frac{u_3}{I_{yy}} + \frac{I_{zz} - I_{xx}}{I_{yy}}pr + \frac{J_{prop}}{I_{yy}}p\omega_p$$

$$\dot{r} = \frac{u_4}{I_{zz}} + \frac{I_{xx} - I_{yy}}{I_{zz}}pq \tag{2.27}$$

where $\omega_p = \omega_1 - \omega_2 - \omega_3 + \omega_4$.

For the transition and the horizontal flight modes, dynamics of the aerial vehicle can be written as

$$\ddot{X} = \frac{1}{m}[(c_\psi c_\theta c_{\theta_f} - (c_\phi s_\theta c_\psi + s_\phi s_\psi)s_{\theta_f})u_1 + W_x]$$

$$\ddot{Y} = \frac{1}{m}[(s_\psi c_\theta c_{\theta_f} - (c_\phi s_\theta s_\psi - s_\phi c_\psi)s_{\theta_f})u_1 + W_y]$$

$$\ddot{Z} = \frac{1}{m}[(-s_\theta c_{\theta_f} - c_\phi c_\theta s_{\theta_f})u_1 + mg + W_z]$$

$$\dot{p} = \frac{u_2}{I_{xx}} + \frac{I_{yy} - I_{zz}}{I_{xx}}qr - \frac{J_{prop}}{I_{xx}}q\omega_p s_{\theta_f}$$

$$\dot{q} = \frac{u_3}{I_{yy}} + \frac{I_{zz} - I_{xx}}{I_{yy}}pr + \frac{J_{prop}}{I_{yy}}(ps_{\theta_f} + rc_{\theta_f})\omega_p + W_t$$

$$\dot{r} = \frac{u_4}{I_{zz}} + \frac{I_{xx} - I_{yy}}{I_{zz}}pq - \frac{J_{prop}}{I_{zz}}q\omega_p c_{\theta_f} \tag{2.28}$$

For the attitude control, the attitude dynamics of the aerial vehicle must be expressed in the world frame. To this end, rotational part of rigid body

dynamics given in Eqn. (2.8) can be rewritten as

$$\dot{\Omega}_b = I_b^{-1}(-\Omega_b \times (I_b\Omega_b) + M_t) \tag{2.29}$$

and the derivative of Eqn. (2.7) is

$$\dot{\Omega}_w = \dot{\mathbb{B}}\Omega_b + \mathbb{B}\dot{\Omega}_b \tag{2.30}$$

By using Eqn. (2.5) and substituting Eqn. (2.29) into Eqn. (2.30), the equation becomes

$$\dot{\Omega}_w = \dot{\mathbb{B}}\mathbb{E}\Omega_w - \mathbb{B}I_b^{-1}(\mathbb{E}\Omega_w \times I_b\mathbb{E}\Omega_w) + \mathbb{B}I_b^{-1}M_t \tag{2.31}$$

Multiplying both sides of Eqn. (2.31) by the transformed inertia matrix $\mathbb{M}(\alpha_w) = \mathbb{E}^T I_b \mathbb{E}$ and using the fact that $\dot{\mathbb{E}} = -\mathbb{E}\dot{\mathbb{B}}\mathbb{E}$ (see Appendix B for the derivation), the following equation is obtained.

$$\mathbb{M}(\alpha_w)\dot{\Omega}_w = -\mathbb{E}^T I_b \dot{\mathbb{E}}\Omega_w - \mathbb{E}^T(\mathbb{E}\Omega_w \times I_b\mathbb{E}\Omega_w) + \mathbb{E}^T M_t \tag{2.32}$$

Coriolis terms in above equation can be casted into the matrix $\mathbb{C}$ as

$$\mathbb{C}(\alpha_w, \Omega_w) = \mathbb{E}^T I_b \dot{\mathbb{E}} + \mathbb{E}^T S(\mathbb{E}\Omega_w) I_b \mathbb{E}$$

where $S(.)$ is the skew-symmetric matrix that replaces the cross-product. The attitude dynamics expressed in the world frame can be written in a more compact form as follows

$$\mathbb{M}(\alpha_w)\dot{\Omega}_w + \mathbb{C}(\alpha_w, \Omega_w)\Omega_w = \mathbb{E}^T M_t \tag{2.33}$$

The physical parameters of the aerial vehicle are tabulated in Table 2.1.

Table 2.1: Modeling parameters

Symbol	Description	Magnitude
m	mass	4.5 kg
l_s	rotor distance to cog along y axis	0.3 m
l_l	rotor distance to cog along x axis	0.3 m
I_{xx}	moment of inertia along x axis	0.405 kgm^2
I_{yy}	moment of inertia along y axis	0.405 kgm^2
I_{zz}	moment of inertia along z axis	0.72 kgm^2
$\lambda_{1,4}$	torque/force ratio	0.01 Nm/N
$\lambda_{2,3}$	torque/force ratio	-0.01 Nm/N

Chapter III

3   Flight Control System of SUAVI

SUAVI has two fundamental flight modes, which are the vertical and horizontal flights, and a transition mode that is intermediate flight mode between horizontal and vertical flights. During takeoff, landing and hover the wings are in vertical position with respect to the ground, whereas they are tilted between $0° - 90°$ when forward motion is required or in the transition mode (Fig. 3.1). The determination of the tilt angle is based on the requirements
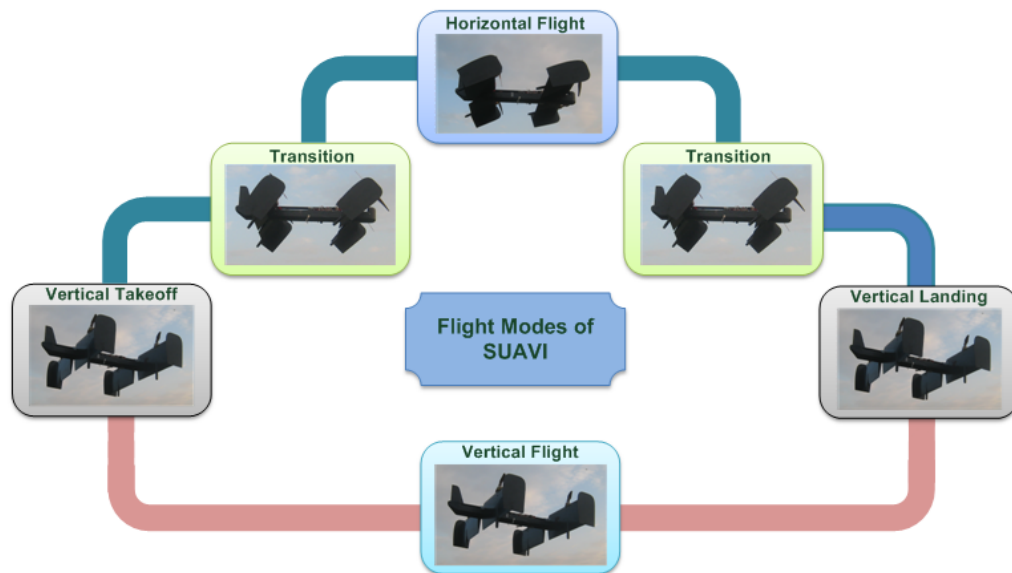

Figure 3.1: Two main flight paths of SUAVI

of the corresponding flight speed. The control system needs to handle all of these issues for accomplishing the stable flight and successful reference tracking.

3.1 Hierarchical Control Architecture

In order to cope with these fundamental issues arising from complex structure of SUAVI, a hierarchical control system (Fig. 3.2) is developed. The high-level controller (supervisor) is responsible for generating feasible trajectories based on GPS and camera data, generating corresponding attitude references for the low-level controllers, switching of the low-level controllers into the closed-loop system depending on the flight mode, forming the communication link with the ground station and performing all checks including security. In case of an emergency such as the lost of the balance of the air vehicle in the transition and horizontal flights, this high level control immediately switches the air vehicle back into the vertical flight configuration to prevent any crashes. (see details in [65, 66]) The low-level controllers are responsible
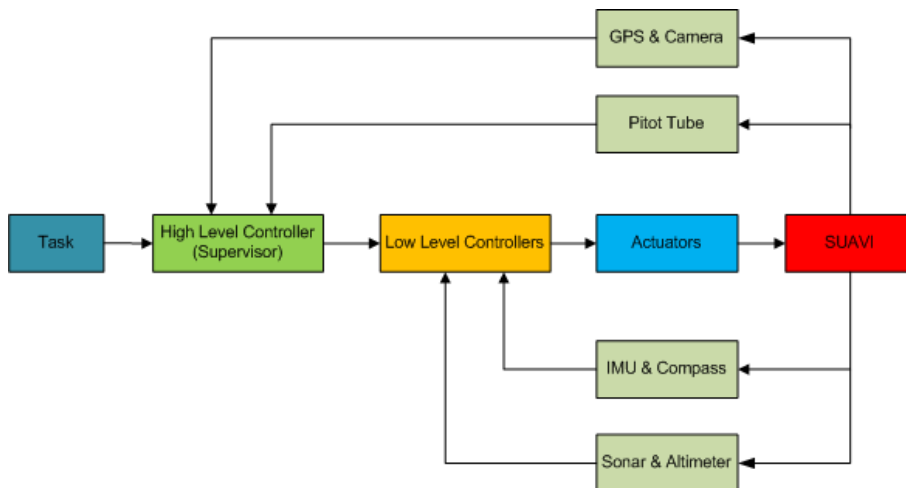

Figure 3.2: Hierarchical control architecture

for obtaining sensor measurements, performing necessary filtering for reliable state estimations, gathering the human operator inputs on the system and handling the low-level control calculations.

3.1.1 Control System Hardware

The electronic flight control system of SUAVI utilizes various sensors for situational awareness, actuators to apply the required control efforts on the plant and several filters to make the sensor data more accurate and reliable.

The high-level controller in the hierarchical control system of SUAVI is implemented in a *Gumstix*® microcomputer. As the high-level controller, Gumstix utilizes data from the GPS and the camera that is connected to the camera port of OMAP3530 processor. The image processing based operations are performed using the OpenCV library. The DSP core on the microcomputer allows the computations of image processing algorithms at higher speeds due to its high computational power (see details in [67]).

The low-level control circuit that is realized for SUAVI is based on three Atmel Atmega16 microcontrollers. These microcontrollers are given separate tasks that are hard real-time, soft real-time or sporadic tasks. This separation guarantees the operation of the 100 Hz hard real-time control loop without missing any deadline.

3.1.1.1 Sensors

To achieve satisfactory stabilization and trajectory tracking tasks, reliable state estimates need to be acquired by the hierarchical control system. For obtaining these reliable state estimates, various sensors are utilized in SUAVI. A Sparkfun 6 DOF v4 inertial measurement unit (IMU) is utilized for the

estimation of roll, pitch, yaw angles and angular velocities through its 3-axis accelerometer, 3-axis gyro, 3-axis magnetometer. It is placed on the aerial vehicle's center of mass to obtain more accurate attitude information. A Honeywell HMC6343 tilt-compensated magnetometer is included in the system for reliable heading measurements. For above the ground altitude measurement, a Maxbotix EZ4 sonar with 2.54 cm ($1''$) of resolution for up to 6.45 m distance is used and a VTI Technologies SCP1000 altimeter with 10 cm resolution is utilized for higher altitude measurements. For the horizontal airspeed measurements an Eagle Tree Airspeed MicroSensor V3 with pitot tube is embedded to the system. An ADH Technology D2523T GPS unit with a high-gain active antenna and 50 channel GPS receiver circuits, which can deliver 2 Hz GPS data is embedded in the system for world coordinate estimations. Moreover, in order to obtain reliable feedback signals for flight control system, several analog and digital filters such as extended Kalman filter, analog anti-aliasing filter and digital exponentially weighted moving average filter are also implemented in the control system of SUAVI (see details in [65]). Hardware implementation layout together with the hierarchical control architecture is depicted in Fig. 3.3.

3.1.1.2 Actuators

To apply the forces demanded by the control system for the stable flight of SUAVI in all possible flight conditions, reliable and highly capable actuators are required. Great Planes Rimfire 42-40-800 is chosen among a variety of RC aircraft electric motors for propulsion, since it is a high efficiency direct drive brushless motor. It can deliver more than 1.6 kg of thrust with 14x7 inch propellers. For controlling the motor speeds, Great Planes Electrifly Silver
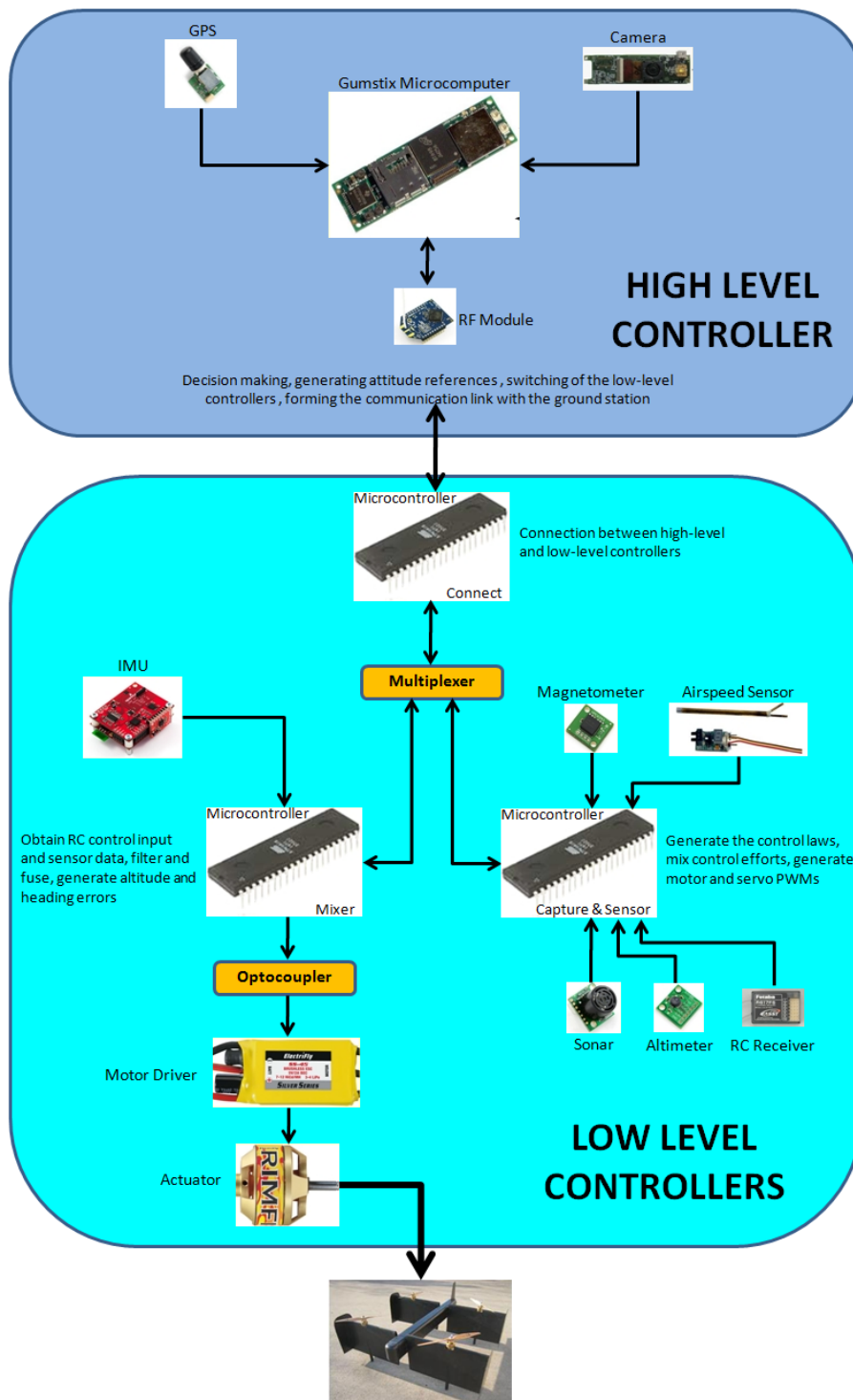
GPS

Camera

Gumstix Microcomputer

RF Module

HIGH LEVEL CONTROLLER

Decision making, generating attitude references , switching of the low-level controllers , forming the communication link with the ground station

Microcontroller

Connection between high-level and low-level controllers

Connect

IMU

Multiplexer

Magnetometer

Airspeed Sensor

Microcontroller

Obtain RC control input and sensor data, filter and fuse, generate altitude and heading errors

Mixer

Microcontroller

Generate the control laws, mix control efforts, generate motor and servo PWMs

Capture & Sensor

Optocoupler

Sonar

Altimeter

RC Receiver

Motor Driver

Actuator

LOW LEVEL CONTROLLERS

Figure 3.3: Flight Control System Implementation on the Hardware

Series 35 motor driver is preferred, which is capable of delivering up to 35 A continuously, where the maximum allowed current of the chosen motor is 32 A. For tilting the wings in the horizontal-vertical range, TS170 high torque digital RC servos with 18 kgcm torque and titanium gears are utilized. They are deliberately chosen that way to ensure very robust wing orientation even in the existence of disturbances of wind gusts and also during landing.

3.2 Flight Control System Design

In order to design flight controllers, i.e. position and attitude controllers, of vertical, transition and horizontal modes, dynamics of aerial vehicle is divided into two subsystems, namely position and attitude subsystems [68]. Since the position subsystem has slow dynamics, this subsystem is utilized to create reference angles for the attitude subsystem by exploiting the structure of the position subsystem. For simplicity, the downwash effects of the front wings on rear wings will be neglected, therefore equal front and rear wing angles will be assumed, i.e $\theta_f = \theta_r$. Control calculations will be based on front wing angles. A development without this assumption will be much more involved. However, it should be noted that in practical flight tests a look-up table which is obtained from the wind tunnel tests is used by the high level controller to command the servos to place the rear wings at a higher angle of attack than the front wings.

3.2.1 Vertical Mode Position Controllers

For the vertical mode position control of SUAVI, two different nonlinear control approaches are proposed, namely integral sliding mode and PID based controllers. Both control techniques utilizes the nonlinear transformation

based on dynamic inversion method and generate reference angles for the attitude subsystems.

3.2.1.1 PID Based Controllers via Dynamic Inversion

In order to design vertical mode position controllers, first the aerial vehicle position (X, Y and Z) dynamics is recalled; i.e

$$\ddot{X} = \frac{1}{m}[(c_\psi c_\theta c_{\theta_f} - (c_\phi s_\theta c_\psi + s_\phi s_\psi)s_{\theta_f})u_1 + W_x] \tag{3.1}$$

$$\ddot{Y} = \frac{1}{m}[(s_\psi c_\theta c_{\theta_f} - (c_\phi s_\theta s_\psi - s_\phi c_\psi)s_{\theta_f})u_1 + W_y] \tag{3.2}$$

$$\ddot{Z} = \frac{1}{m}[(-s_\theta c_{\theta_f} - c_\phi c_\theta s_{\theta_f})u_1 + mg + W_z] \tag{3.3}$$

The aerial vehicle has to produce required accelerations along X, Y and Z axis, in order to track the desired trajectory in vertical mode. These accelerations can be generated by virtual control inputs which are designed as PID controllers; i.e.

$$\mu_1 = K_{p_x}e_x + K_{ix}\int_0^t e_x dt + K_{dx}\dot{e}_x \tag{3.4}$$

$$\mu_2 = K_{p_y}e_y + K_{iy}\int_0^t e_y dt + K_{dy}\dot{e}_y \tag{3.5}$$

$$\mu_3 = K_{p_z}e_z + K_{iz}\int_0^t e_z dt + K_{dz}\dot{e}_z \tag{3.6}$$

where position tracking errors are defined as $e_q = q_d - q$ for $q = X, Y, Z$. The aerial vehicle is required to track the desired attitude angles and produce the total thrust to generate the desired acceleration. In order to compute these desired attitude angles and the total thrust, dynamic inversion approach can be utilized. By equating virtual control inputs to position dynamics

44

and transferring gravity and aerodynamic forces to the left hand side of the equation, the following equations are obtained

$$\tilde{\mu}_1 \triangleq m\mu_1 - W_x = (c_{\psi_d}c_{\theta_d}c_{\theta_f} - (c_{\phi_d}s_{\theta_d}c_{\psi_d} + s_{\phi_d}s_{\psi_d})s_{\theta_f})u_1 \qquad (3.7)$$

$$\tilde{\mu}_2 \triangleq m\mu_2 - W_y = (s_{\psi_d}c_{\theta_d}c_{\theta_f} - (c_{\phi_d}s_{\theta_d}s_{\psi_d} - s_{\phi_d}c_{\psi_d})s_{\theta_f})u_1 \qquad (3.8)$$

$$\tilde{\mu}_3 \triangleq m\mu_3 - W_z - mg = (-s_{\theta_d}c_{\theta_f} - c_{\phi_d}c_{\theta_d}s_{\theta_f})u_1 \qquad (3.9)$$

where $\tilde{\mu}_1$, $\tilde{\mu}_2$ and $\tilde{\mu}_3$ are new virtual inputs. Equations (3.7)-(3.9) can be solved for the total thrust u_1, desired roll (ϕ_d) and pitch (θ_d) angles as (see details in Appendix C)

$$u_1 = \sqrt{\tilde{\mu}_1^2 + \tilde{\mu}_2^2 + \tilde{\mu}_3^2} \qquad (3.10)$$

$$\phi_d = \arcsin(\frac{\gamma_2}{u_1 \cdot s_{\theta_f}}) \qquad (3.11)$$

$$\theta_d = \arcsin(\frac{-\tilde{\mu}_3 \cdot u_1 \cdot c_{\theta_f} - u_1 \cdot \gamma_1 \cdot s_{\theta_f} \cdot c_{\phi_d}}{\gamma_1{}^2 + \tilde{\mu}_3^2}) \qquad (3.12)$$

where γ_1 and γ_2 are the auxiliary variables and they are defined as

$$\gamma_1 = \tilde{\mu}_1 \cdot c_{\psi_d} + \tilde{\mu}_2 \cdot s_{\psi_d} \qquad (3.13)$$

$$\gamma_2 = \tilde{\mu}_1 \cdot s_{\psi_d} - \tilde{\mu}_2 \cdot c_{\psi_d} \qquad (3.14)$$

Desired roll and pitch angles computed using Eqns. (3.11) and (3.12) will be references for the attitude subsystem. It should be noted that the desired yaw angle can be set to any reference value. Note that the total thrust and the desired attitude angles are functions of the wing angles ($\theta_f = \theta_r$). In the literature there exists such reference angle calculations for quadrotors [68], however calculations that depend on wing angles are not studied for tilt-wing

or tilt-rotor quadrotors. Our developments here provide reference angles for quadrotors that have tilted wings or rotors.

Remark: SUAVI behaves like a quadrotor when the wing angles are set to an angle higher than 70° (tilted 20° from the vertical). To see this, recall that $\sin(70) \approx 0.94$ and therefore the vertical thrust component dominates the horizontal one.

3.2.1.2 Integral Sliding Mode Controllers via Dynamic Inversion

In this section, instead of PID based controllers, integral sliding mode control will be utilized to design virtual control inputs and the designed virtual control inputs will again be used in the dynamic inversion approach. The advantage of sliding mode control is its insensitivity to the model errors, parametric uncertainties and other disturbances. These robustness against uncertainties and disturbances can only be realized after the system is confined to the sliding manifold. Therefore the conventional sliding mode control cannot assure the robustness during the reaching phase. However, integral sliding mode [69] control can achieve elimination of the reaching phase, hence robustness of the system is attained by enforcing the sliding mode throughout the entire system response. In order to design integral sliding mode control, position dynamics can be rewritten as

$$\mathbb{G}\dot{V}_w + \mathbb{H} = \mathcal{F} \tag{3.15}$$

where aerial vehicle's mass matrix, external forces, disturbance and gravity vector are casted into new variables as follows:

$$\mathbb{G} \triangleq mI_{3\times3} \tag{3.16}$$

$$\mathbb{H} \triangleq R_{wb}(F_w + F_d + F_g) \tag{3.17}$$

$$F = \begin{bmatrix} F_1 & F_2 & F_3 \end{bmatrix}^T \triangleq R_{wb}F_{th} \tag{3.18}$$

For the position dynamics the ideal control law, which employs nominal parameters of the position dynamics, can achieve the zero tracking error, if there does not exist any parameter uncertainty and disturbances. Among many other ideal control techniques, inverse dynamics control is one of the most commonly used control technique in robotics area. The main idea behind inverse dynamics control is to transform dynamical system into only an acceleration dynamics by canceling mass-inertia terms, coriolis terms, gravity terms, etc. By utilizing this control approach, the nominal control input $\widehat{F}$ can be computed as

$$\widehat{F} = \widehat{\mathbb{G}}(\dot{V}_w^d - K_{dps}\dot{e}_{ps} - K_{p_{ps}}e_{ps}) + \widehat{\mathbb{H}} \tag{3.19}$$

where $\dot{V}_w^d = [\ddot{X}_d \quad \ddot{Y}_d \quad \ddot{Z}_d]^T$ is the vector that contains desired linear accelerations, $K_{p_{ps}}$ and $K_{d_{ps}}$ are 3×3 positive definite diagonal gain matrices, $\widehat{\mathbb{G}}$ and $\widehat{\mathbb{H}}$ are the nominal values of $\mathbb{G}$ matrix and $\mathbb{H}$ vector. The error vector and its derivative appear in above equation are defined as

$$e_{ps} = \begin{bmatrix} X - X_d \\ Y - Y_d \\ Z - Z_d \end{bmatrix}, \quad \dot{e}_{ps} = \begin{bmatrix} \dot{X} - \dot{X}_d \\ \dot{Y} - \dot{Y}_d \\ \dot{Z} - \dot{Z}_d \end{bmatrix} \tag{3.20}$$

If the parameters of the position dynamics are exactly known, i.e. $\mathbb{G} = \widehat{\mathbb{G}}$ and $\mathbb{H} = \widehat{\mathbb{H}}$, the closed-loop error dynamics can be calculated by substituting Eqn. (3.19) into Eqn. (3.15):

$$\ddot{e}_{ps} + K_{dps}\dot{e}_{ps} + K_{pps}e_{ps} = 0 \qquad (3.21)$$

Hence error goes to zero as $t \to \infty$. However, due to disturbances acting on the system, uncertainties in plant parameters, and estimation errors in the lift and drag forces the error dynamics becomes

$$\ddot{e}_{ps} + K_{dps}\dot{e}_{ps} + K_{pps}e_{ps} = \widehat{\mathbb{G}}^{-1}(\widetilde{\mathbb{G}}\dot{V}_w + \widetilde{\mathbb{H}}) \qquad (3.22)$$

where $\widetilde{\mathbb{G}} = \widehat{\mathbb{G}} - \mathbb{G}$ and $\widetilde{\mathbb{H}} = \widehat{\mathbb{H}} - \mathbb{H}$ are the parameter errors. As Eqn. (3.22) indicates, the existence of parameter errors prevents position error from going to zero. Hence, a robust control scheme is required to achieve zero tracking error. To this end, integral sliding mode control will be designed. The control input $F = \widehat{F} + F_s$ will consist of the two terms, namely ideal control $\widehat{F}$ and discontinuous control F_s that rejects the total disturbance on the system. In order to design integral sliding mode control, the sliding surface is defined as

$$\sigma = \sigma_0 + z_{ps} \qquad (3.23)$$

where σ_0 is the linear combination of error and its derivative as in the typical sliding mode control and z_{ps} is the term that brings out the integral action. These two terms can be designed as

$$\sigma_0 = K_1 e_{ps} + \dot{e}_{ps} \qquad (3.24)$$

and

$$\dot{z}_{ps} = -K_1 \dot{e}_{ps} + \widehat{\mathbb{G}}^{-1}\widehat{\mathbb{H}} - \widehat{\mathbb{G}}^{-1}\widehat{F} + \dot{V}_w^d \qquad (3.25)$$

with the initial condition

$$\dot{z}_{ps}(0) = -K_1 e_{ps}(0) - \dot{e}_{ps}(0) \qquad (3.26)$$

where K_1 is the positive definite diagonal gain matrix. The initial condition is imposed on $\dot{z}_{ps}$ to eliminate reaching time of sliding surface. By differentiating Eqn. (3.24) and substituting $\dot{V}_w$ with position dynamics given Eqn. (3.15), the derivative of the sliding surface can be computed as

$$\dot{\sigma} = \dot{\sigma}_0 + \dot{z}_{ps} = K_1 \dot{e}_{ps} + \ddot{e}_{ps} - K_1 \dot{e}_{ps} + \widehat{\mathbb{G}}^{-1}\widehat{\mathbb{H}} - \widehat{\mathbb{G}}^{-1}\widehat{F} + \dot{V}_w^d$$

$$\Rightarrow \dot{\sigma} = \dot{V}_w - \dot{V}_w^d + \widehat{\mathbb{G}}^{-1}\widehat{\mathbb{H}} - \widehat{\mathbb{G}}^{-1}\widehat{F} + \dot{V}_w^d = \dot{V}_w + \widehat{\mathbb{G}}^{-1}\widehat{\mathbb{H}} - \widehat{\mathbb{G}}^{-1}\widehat{F}$$

$$\Rightarrow \dot{\sigma} = -\mathbb{G}^{-1}\mathbb{H} + \mathbb{G}^{-1}(\widehat{F} + F_s) + \widehat{\mathbb{G}}^{-1}\widehat{\mathbb{H}} - \widehat{\mathbb{G}}^{-1}\widehat{F}$$

$$\dot{\sigma} = \widehat{\mathbb{G}}^{-1}\widehat{\mathbb{H}} - \mathbb{G}^{-1}\mathbb{H} - (\widehat{\mathbb{G}}^{-1} - \mathbb{G}^{-1})\widehat{F} + \mathbb{G}^{-1}F_s \qquad (3.27)$$

The derivative of the sliding surface can be written in a more compact form by defining new parameter error vector Γ_1 and matrix Γ_2 as

$$\Gamma_1 \triangleq \widehat{\mathbb{G}}^{-1}\widehat{\mathbb{H}} - \mathbb{G}^{-1}\mathbb{H}, \quad \Gamma_2 \triangleq \widehat{\mathbb{G}}^{-1} - \mathbb{G}^{-1} \qquad (3.28)$$

Therefore the derivative of the sliding surface is

$$\dot{\sigma} = \Gamma_1 - \Gamma_2\widehat{F} + \mathbb{G}^{-1}F_s \qquad (3.29)$$

49

Continuous part of the control input $\widehat{F}$ appears in above equation is defined in Eqn. (3.19) which is the ideal control law based on inverse dynamics control approach. In order to reject non-ideal part of system, discontinuous part of the control input is design as in the typical sliding mode control:

$$F_s = -K_2 sign(\sigma) \qquad (3.30)$$

where K_2 is the positive constant gain and $sign(\cdot)$ is the well-known signum function. To determine range of K_2, Lyapunov function candidate can be chosen as

$$V_1 = \frac{1}{2}\sigma^T \sigma \qquad (3.31)$$

and its time derivative can be computed by using Eqns. (3.29) and (3.30) as follows

$$\dot{V}_1 = \sigma^T \dot{\sigma} = \sigma^T(\Gamma_1 - \Gamma_2 \widehat{F}) - \sigma^T(\mathbb{G}^{-1}K_2 sign(\sigma)) \qquad (3.32)$$

In order to achieve finite time convergence and to reach sliding regime, we have to guarantee that $\dot{V}_1 < 0$. By manipulating Eqn. (3.32) and using the fact that $|x| \geq x$, we obtain

$$\dot{V}_1 \leq |\sigma^T(\Gamma_1 - \Gamma_2 \widehat{F})| - \sigma^T(\mathbb{G}^{-1}K_2 sign(\sigma)) < 0 \qquad (3.33)$$

Since the mass matrix $\mathbb{G}$ is a positive definite diagonal matrix, K_2 is a positive constant and $xsign(x) = |x|$, the second part (i.e. $\sigma^T(\mathbb{G}^{-1}K_2 sign(\sigma))$) of the equation is always positive. Hence Eqn. (3.33) can be rewritten as

$$\dot{V} \leq |\sigma^T(\Gamma_1 - \Gamma_2 \widehat{F})| - K_2|\sigma^T(\mathbb{G}^{-1}sign(\sigma))| < 0 \qquad (3.34)$$

By using the fact that $x^T y = \langle x, y \rangle$ and Cauchy-Schwarz inequality, Eqn. (3.34) becomes

$$\dot{V} \leq \|\sigma\| \|(\Gamma_1 - \Gamma_2 \widehat{F})\| - K_2 \|\sigma\| \|\mathbb{G}^{-1}\| < 0 \qquad (3.35)$$

Hence the following constraint must be imposed on K_2 to obtain $\dot{V}_1 < 0$:

$$K_2 > \frac{\|(\Gamma_1 - \Gamma_2 \widehat{F})\|}{\|\mathbb{G}^{-1}\|} \qquad (3.36)$$

When the system reaches to sliding regime and it is restricted in sliding manifold, the equivalent control can be used to investigate behavior of the system. By formally equating $\dot{\sigma} = 0$, the equivalent control F_{seq} can be found as

$$\dot{\sigma} = \Gamma_1 - \Gamma_2 \widehat{F} + \mathbb{G}^{-1} F_{seq} = 0$$

$$\Rightarrow F_{seq} = \mathbb{G}(\Gamma_2 \widehat{F} - \Gamma_1) \qquad (3.37)$$

By substituting $F = \widehat{F} + F_{seq}$ into Eqn. (3.15) and using Eqn. (3.28), dynamic equation of position subsystem can be written as

$$\mathbb{G}\dot{V}_w + \mathbb{H} = \widehat{F} + \mathbb{G}((\widehat{\mathbb{G}}^{-1} - \mathbb{G}^{-1})\widehat{F} - \widehat{\mathbb{G}}^{-1}\widehat{\mathbb{H}} + \mathbb{G}^{-1}\mathbb{H})$$

$$\Rightarrow \mathbb{G}\dot{V}_w + \mathbb{H} = \widehat{F} + \mathbb{G}\widehat{\mathbb{G}}^{-1}\widehat{F} - \widehat{F} - \mathbb{G}\widehat{\mathbb{G}}^{-1}\widehat{\mathbb{H}} + \mathbb{H}$$

$$\Rightarrow \dot{V}_w = \widehat{\mathbb{G}}^{-1}\widehat{F} - \widehat{\mathbb{G}}^{-1}\widehat{\mathbb{H}}$$

$$\Rightarrow \widehat{\mathbb{G}}\dot{V}_w + \widehat{\mathbb{H}} = \widehat{F} \qquad (3.38)$$

Therefore during the sliding regime the ideal control input defined in Eqn. (3.19) can achieve zero tracking error, as if there is no perturbation on the

system. In order to apply this control input to the position subsystem, the derived sliding mode control input can be utilized as virtual control input as in the PID based vertical mode position controllers. To this end, Eqn. (3.18) can be rewritten explicitly as follows

$$F_1 = (c_{\psi_d}c_{\theta_d}c_{\theta_f} - (c_{\phi_d}s_{\theta_d}c_{\psi_d} + s_{\phi_d}s_{\psi_d})s_{\theta_f})u_1 \tag{3.39}$$

$$F_2 = (s_{\psi_d}c_{\theta_d}c_{\theta_f} - (c_{\phi_d}s_{\theta_d}s_{\psi_d} - s_{\phi_d}c_{\psi_d})s_{\theta_f})u_1 \tag{3.40}$$

$$F_3 = (-s_{\theta_d}c_{\theta_f} - c_{\phi_d}c_{\theta_d}s_{\theta_f})u_1 \tag{3.41}$$

Equations (3.39)-(3.41) can again be solved (see Appendix C) for the total thrust u_1, desired roll (ϕ_d) and pitch (θ_d) angles as

$$u_1 = \sqrt{F_1{}^2 + F_2{}^2 + F_3{}^2} \tag{3.42}$$

$$\phi_d = \arcsin(\frac{\gamma_4}{u_1 \cdot s_{\theta_f}}) \tag{3.43}$$

$$\theta_d = \arcsin(\frac{-F_3 \cdot u_1 \cdot c_{\theta_f} - u_1 \cdot \gamma_3 \cdot s_{\theta_f} \cdot c_{\phi_d}}{\gamma_3{}^2 + F_3{}^2}) \tag{3.44}$$

where γ_3 and γ_4 are the auxiliary variables and they are defined as

$$\gamma_3 = F_1 \cdot c_{\psi_d} + F_2 \cdot s_{\psi_d} \tag{3.45}$$

$$\gamma_4 = F_1 \cdot s_{\psi_d} - F_2 \cdot c_{\psi_d} \tag{3.46}$$

Desired roll and pitch angles computed using Eqns. (3.43) and (3.44) will be references for the attitude subsystem. It should be noted that the desired yaw angle can be set to any reference value. Note that the total thrust and the desired attitude angles are again the functions of the wing angles $(\theta_f = \theta_r)$.

3.2.2 Transition Mode Position Controllers

These position controllers are employed during the transition between the vertical ($\theta_f = \theta_r = 90°$) and the horizontal ($\theta_f = \theta_r < 30°$) wing angles. Transition mode of the aerial vehicle has a significant effect on the flight performance. Hence, it must be realized in a very smooth manner without creating an inbalance on the air vehicle. In the transition mode, the aerial vehicle is neither a plane nor a quadrotor helicopter, instead it is a hybrid air vehicle with a complex dynamical model that is highly dependent on the wing angle of attacks. The high level control system gives commands for the front and rear wing angle of attacks and motor PWM values using the tabulated data for the nominal flight according to the measured air speed and the position reference. Since wings are tilted in this flight mode, forward acceleration of the aerial vehicle is produced by horizontal component of the total thrust. The purpose of transition mode position controllers is to keep the altitude of the aerial vehicle at some desired value. By setting $\tilde{\mu}_1 = 0$, the total thrust and the desired roll angle for this flight mode can be computed as

$$u_1 = \sqrt{\tilde{\mu}_2^2 + \tilde{\mu}_3^2} \tag{3.47}$$

$$\phi_d = \arcsin(\frac{-\tilde{\mu}_2 \cdot c_{\psi_d}}{u_1 \cdot s_{\theta_f}}) \tag{3.48}$$

Virtual inputs $\tilde{\mu}_2$ and $\tilde{\mu}_3$ that appear in above equations can be computed by utilizing controllers given in Eqns. (3.5)-(3.6) and (3.8)-(3.9). Calculated desired roll angle is a reference angle for attitude subsystem and it is required to direct motor thrusts. The desired pitch angle is set to zero ($\theta_d = 0$) in order to make the fuselage parallel to the ground and the desired yaw angle

is set arbitrarily in transition mode.

3.2.3 Horizontal Mode Position Controllers

After the wings are tilted to the desired angle, horizontal mode position controllers are activated. In this flight mode acceleration along Z direction is produced by vertical component of the total thrust which is created by tilted wings. The purpose of the horizontal flight mode is to track given trajectory along X and Y axes. For the trajectory tracking along X axis the total thrust will be used. For the tracking along Y axis the vertical component of the total thrust is directed by rolling the aerial vehicle. In order to design the controller for X axis and compute the total thrust, dynamics of X can be linearized as

$$\ddot{X} = \frac{1}{m}(u_1 c_{\theta_f} + W_x) \tag{3.49}$$

The following PID controller is designed for the linearized dynamics:

$$u_1 = K_{p_x} e_x + K_{i_x} \int_0^t e_x dt + K_{d_x} \dot{e}_x - \frac{W_x}{c_{\theta_f}} \tag{3.50}$$

where position tracking error is defined as $e_x = X_d - X$. As in vertical mode, the total thrust is directed by rolling the aerial vehicle. Desired roll angle can again be computed using Eqn. (3.48). But in this case, the total thrust u_1 is calculated from Eqn. (3.50). Similar to the transition mode, desired roll angle is a reference angle for attitude subsystem and desired pitch angle is set to zero ($\theta_d = 0$) in order to make the fuselage parallel to the ground. Yaw angle reference is given arbitrarily in horizontal mode.

3.2.4 Attitude Controllers

For the attitude control of SUAVI, two different nonlinear control approaches are proposed, namely feedback linearization and integral sliding mode attitude controllers. These attitude controllers are the same for all three flight modes. Desired attitude angles given in Sections $3.2.1 - 3.2.3$ are used as the reference angles.

3.2.4.1 Feedback Linearization Attitude Controllers

To design feedback linearization attitude controllers, Eqn. (2.33) can be rewritten as

$$\mathbb{M}(\alpha_w)\dot{\Omega}_w + \mathbb{C}(\alpha_w, \Omega_w)\Omega_w = \mathbb{E}^T(M_{th} + M_w) \qquad (3.51)$$

where $M_t \approx M_{th} + M_w$. Note that gyroscopic effects included in M_t are neglected. Since gyroscopic effects on propellers are small enough to be neglected, these moments are not considered in controller design. The attitude dynamics given in Eqn. (3.65) is fully actuated, therefore it is feedback linearizable. Consider the following transformation for feedback linearization:

$$\tilde{\eta} = M_{th} = I_b \mathbb{E} \eta + \mathbb{E}^{-T}\mathbb{C}(\alpha_w, \Omega_w)\Omega_w - M_w \qquad (3.52)$$

where $\tilde{\eta}$ is a new virtual control input vector and η is the virtual control input vector for attitude subsystem. These control inputs have 3 components and they are defined as

$$\tilde{\eta} = \begin{bmatrix} \tilde{\eta}_1 & \tilde{\eta}_2 & \tilde{\eta}_3 \end{bmatrix}^T, \quad \eta = \begin{bmatrix} \eta_1 & \eta_2 & \eta_3 \end{bmatrix}^T \qquad (3.53)$$

In light of Eqns. (2.22), (3.52) and (3.53), it follows that

$$\tilde{\eta}_1 = s_{\theta_f} u_2 - c_{\theta_f} u_4 \tag{3.54}$$

$$\tilde{\eta}_2 = s_{\theta_f} u_3 \tag{3.55}$$

$$\tilde{\eta}_3 = c_{\theta_f} u_2 + s_{\theta_f} u_4 \tag{3.56}$$

The following PID controllers are designed to generate virtual control inputs, η_1, η_2, η_3; i.e.

$$\eta_1 = K_{p_\phi} e_\phi + K_{i\phi} \int_0^t e_\phi dt + K_{d\phi} \dot{e}_\phi \tag{3.57}$$

$$\eta_2 = K_{p\theta} e_\theta + K_{i\theta} \int_0^t e_\theta dt + K_{d\theta} \dot{e}_\theta \tag{3.58}$$

$$\eta_3 = K_{p\psi} e_\psi + K_{i\psi} \int_0^t e_\psi dt + K_{d\psi} \dot{e}_\psi \tag{3.59}$$

where attitude tracking errors are defined as $e_q = q_d - q$ for $q = \phi, \theta, \psi$. It should again be emphasized that in vertical flight mode desired roll and pitch angles (ϕ_d, θ_d) are computed from position subsystem, whereas in transition and horizontal flight mode only desired roll angle is computed from position subsystem. Pitch angle reference for transition and horizontal mode is set to $\theta_d = 0$. On the other hand, the desired yaw angle is specified by the user or the high level controller for all three flight modes.

It is well known that physical inputs for quadrotor type aerial vehicles are rotor rotational speeds that generate motor thrusts. The relationship between control inputs and rotor speeds is given through Eqns. (2.23)-(2.26). The total thrust u_1 generated by rotors is given in Eqns. (3.10) (or in Eqn. (3.42) for integral sliding mode controllers), (3.47) and (3.50) for vertical,

transition and horizontal modes, respectively. In light of Eqns. (3.54)-(3.56), the other control inputs u_{2-4} can easily be found as

$$u_3 = \frac{\tilde{\eta}_2}{s_{\theta_f}} \tag{3.60}$$

$$\begin{bmatrix} u_2 \\ u_4 \end{bmatrix} = \begin{bmatrix} s_{\theta_f} & -c_{\theta_f} \\ c_{\theta_f} & s_{\theta_f} \end{bmatrix}^{-1} \begin{bmatrix} \tilde{\eta}_1 \\ \tilde{\eta}_3 \end{bmatrix} \tag{3.61}$$

3.2.4.2 Integral Sliding Mode Attitude Controllers

In this section, instead of feedback linearization controllers, integral sliding mode control will be utilized to design attitude controllers. The attitude dynamics of the aerial vehicle in world frame is derived in Section 2.2 and can be given as

$$\mathbb{M}(\alpha_w)\dot{\Omega}_w + \mathbb{C}(\alpha_w, \Omega_w)\Omega_w = \mathbb{E}^T M_t \tag{3.62}$$

To design integral sliding mode attitude controllers, coriolis terms, gyroscopic effects, moments due to aerodynamic forces and moments due to motor thrusts can be casted into new variables $\mathbb{N}$ and τ as follows

$$\mathbb{N} \triangleq \mathbb{C}(\alpha_w, \Omega_w) - \mathbb{E}^T(M_{gyro} + M_w) \tag{3.63}$$

$$\tau \triangleq \mathbb{E}^T M_t \tag{3.64}$$

Therefore attitude dynamics in terms of new variables can be written as

$$\mathbb{M}\dot{\Omega}_w + \mathbb{N} = \tau \tag{3.65}$$

57

For the attitude dynamics the ideal control law, which is based on inverse dynamics control, can achieve the zero tracking error in the absence of parameter uncertainties and external disturbances. By utilizing inverse dynamics control approach, the nominal control input for the attitude subsystem can be obtained as

$$\widehat{\tau} = \widehat{\mathbb{M}}(\dot{\Omega}_w^d - K_{d_{at}}\dot{e}_{at} - K_{p_{at}}e_{at}) + \widehat{\mathbb{N}} \tag{3.66}$$

where $\dot{\Omega}_w^d = [\ddot{\phi}_d \quad \ddot{\theta}_d \quad \ddot{\psi}_d]^T$ is the vector that contains second derivatives of desired attitude angles, $K_{p_{at}}$ and $K_{d_{at}}$ are 3×3 positive definite diagonal gain matrices, $\widehat{\mathbb{M}}$ and $\widehat{\mathbb{N}}$ are the nominal values of $\mathbb{M}$ matrix and $\mathbb{N}$ vector. The error vector and its derivative are defined as

$$e_{at} = \begin{bmatrix} \phi - \phi_d \\ \theta - \theta_d \\ \psi - \psi_d \end{bmatrix}, \quad \dot{e}_{at} = \begin{bmatrix} \dot{\phi} - \dot{\phi}_d \\ \dot{\theta} - \dot{\theta}_d \\ \dot{\psi} - \dot{\psi}_d \end{bmatrix} \tag{3.67}$$

If the parameters of the attitude dynamics are exactly known, the closed-loop error dynamics can be calculated by substituting Eqn. (3.66) into Eqn. (3.62):

$$\ddot{e}_{at} + K_{d_{at}}\dot{e}_a + K_{p_{at}}e_{at} = 0 \tag{3.68}$$

Therefore attitude tracking error goes to zero as $t \rightarrow \infty$. However, due to estimation errors and disturbances, the error dynamics becomes

$$\ddot{e}_{at} + K_{d_{at}}\dot{e}_{at} + K_{p_{at}}e_{at} = \widehat{\mathbb{M}}^{-1}(\widetilde{\mathbb{M}}\dot{\Omega}_w + \widetilde{\mathbb{N}}) \tag{3.69}$$

where $\widetilde{\mathbb{M}} = \widehat{\mathbb{M}} - \mathbb{M}$ and $\widetilde{\mathbb{N}} = \widehat{\mathbb{N}} - \mathbb{N}$ are the parameter errors. Therefore integral sliding mode control will be designed to achieve robust control scheme. The

control input $\tau = \widehat{\tau} + \tau_s$ will consist of the two terms, namely ideal control $\widehat{\tau}$ and discontinuous control τ_s. In order to design integral sliding mode attitude controllers, the sliding surface is defined as

$$s = s_0 + z_{at} \tag{3.70}$$

where s_0 is the linear combination of error and its derivative and z_{at} is integral term. These two terms are designed as

$$s_0 = K_3 e_{at} + \dot{e}_{at} \tag{3.71}$$

and

$$\dot{z}_{at} = -K_3 \dot{e}_{at} + \widehat{\mathbb{M}}^{-1}\widehat{\mathbb{N}} - \widehat{\mathbb{M}}^{-1}\widehat{\tau} + \dot{\Omega}_w^d \tag{3.72}$$

with the initial condition

$$\dot{z}_{at}(0) = -K_3 e_{at}(0) - \dot{e}_{at}(0) \tag{3.73}$$

where K_3 is the positive definite diagonal gain matrix. By differentiating Eqn. (3.71) and substituting $\dot{\Omega}_w$ with attitude dynamics given Eqn. (3.62), the derivative of the sliding surface can be obtained as

$$\dot{s} = \widehat{\mathbb{M}}^{-1}\widehat{\mathbb{N}} - \mathbb{M}^{-1}\mathbb{N} - (\widehat{\mathbb{M}}^{-1} - \mathbb{M}^{-1})\widehat{\tau} + \mathbb{M}^{-1}\tau_s \tag{3.74}$$

To rewrite the derivative of the sliding surface in more compact form, new parameter error vector Γ_3 and matrix Γ_4 can be defined as

$$\Gamma_3 \triangleq \widehat{\mathbb{M}}^{-1}\widehat{\mathbb{N}} - \mathbb{M}^{-1}\mathbb{N}, \quad \Gamma_4 \triangleq \widehat{\mathbb{M}}^{-1} - \mathbb{M}^{-1} \tag{3.75}$$

59

Therefore the derivative of the sliding surface is

$$\dot{s} = \Gamma_3 - \Gamma_4\widehat{\tau} + \mathbb{M}^{-1}\tau_s \qquad (3.76)$$

Continuous part of the control input $\widehat{\tau}$ appears in above equation is defined in Eqn. (3.64) which is the ideal control law based on inverse dynamics control approach. In order to reject non-ideal part of system, discontinuous part of the control input is designed as

$$\tau_s = -K_4 sign(s) \qquad (3.77)$$

where K_4 is the positive constant gain and $sign(\cdot)$ is the well-known signum function. To determine range of K_4, Lyapunov function candidate can be chosen as

$$V_2 = \frac{1}{2}s^T s \qquad (3.78)$$

and its time derivative can be computed by using Eqns. (3.76) and (3.77) as follows

$$\dot{V}_2 = s^T\dot{s} = s^T(\Gamma_3 - \Gamma_4\widehat{\tau}) - s^T(\mathbb{M}^{-1}K_4 sign(s)) \qquad (3.79)$$

In order to achieve finite time convergence and reach sliding regime, we have to guarantee that $\dot{V}_2 < 0$. By manipulating Eqn. (3.79) as in Section 3.2.1.2, the following constraint is obtained for K_4:

$$K_4 > \frac{\|(\Gamma_3 - \Gamma_4\widehat{\tau})\|}{\|\mathbb{M}^{-1}\|} \qquad (3.80)$$

To examine behavior of the system which is restricted in sliding manifold, the equivalent control can be found by formally equating $\dot{s} = 0$; i.e.

$$\dot{s} = \Gamma_3 - \Gamma_4 \widehat{\tau} + \mathbb{M}^{-1} \tau_{seq} = 0$$

$$\Rightarrow \tau_{seq} = \mathbb{M}(\Gamma_4 \widehat{\tau} - \Gamma_3) \tag{3.81}$$

By substituting $\tau = \widehat{\tau} + \tau_{seq}$ into Eqn. (3.65) and using Eqn. (3.75), dynamic equation of attitude subsystem can be written as

$$\mathbb{M}\dot{\Omega}_w + \mathbb{N} = \widehat{\tau} + \mathbb{M}((\widehat{\mathbb{M}}^{-1} - \mathbb{M}^{-1})\widehat{\tau} - \widehat{\mathbb{M}}^{-1}\widehat{\mathbb{N}} + \mathbb{M}^{-1}\mathbb{N})$$

$$\Rightarrow \mathbb{M}\dot{\Omega}_w + \mathbb{N} = \widehat{\tau} + \mathbb{M}\widehat{\mathbb{M}}^{-1}\widehat{\tau} - \widehat{\tau} - \mathbb{M}\widehat{\mathbb{M}}^{-1}\widehat{\mathbb{N}} + \mathbb{N}$$

$$\Rightarrow \dot{\Omega}_w = \widehat{\mathbb{M}}^{-1}\widehat{\tau} - \widehat{\mathbb{M}}^{-1}\widehat{\mathbb{N}}$$

$$\Rightarrow \widehat{\mathbb{M}}\dot{\Omega}_w + \widehat{\mathbb{N}} = \widehat{\tau} \tag{3.82}$$

Therefore the ideal control input defined in Eqn. (3.66) can achieve zero tracking error, as if there is no perturbation on the system. In order to apply this control input to the attitude subsystem, the derived integral sliding mode control input can be utilized as virtual control input as in the feedback linearization controllers. Hence, by defining virtual control input as

$$\bar{\tau} = \begin{bmatrix} \bar{\tau}_1 & \bar{\tau}_2 & \bar{\tau}_3 \end{bmatrix}^T \triangleq \mathbb{E}^{-T}\tau$$

and using Eqn. (2.22), following equalities for attitude subsystem can be obtained:

$$\bar{\tau}_1 = s_{\theta_f} u_2 - c_{\theta_f} u_4 \tag{3.83}$$

$$\bar{\tau}_2 = s_{\theta_f} u_3 \tag{3.84}$$

$$\bar{\tau}_3 = c_{\theta_f} u_2 + s_{\theta_f} u_4 \tag{3.85}$$

61

In light of Eqns. (3.83)-(3.85), the control inputs u_{2-4} can easily be found as

$$u_3 = \frac{\bar{\tau}_2}{s_{\theta_f}} \tag{3.86}$$

$$\begin{bmatrix} u_2 \\ u_4 \end{bmatrix} = \begin{bmatrix} s_{\theta_f} & -c_{\theta_f} \\ c_{\theta_f} & s_{\theta_f} \end{bmatrix}^{-1} \begin{bmatrix} \bar{\tau}_1 \\ \bar{\tau}_3 \end{bmatrix} \tag{3.87}$$

Chapter IV

4 Simulations and Experimental Results

In order to verify proposed control methods, several simulations are carried out in Matlab/Simulink environment. After successful simulations results are attained, the proposed control methods are implemented on the electronic control system of the aerial vehicle and real flight experiments are conducted.

4.1 Simulations Results

4.1.1 Vertical Mode Flight Controllers

For the vertical flight mode of the aerial vehicle two nonlinear position controllers together with attitude controllers are designed in Chapter 3. In this section, performance of the integral sliding mode position and attitude controllers will be compared with performance of the PID based position and feedback linearization attitude controllers.

In the first simulation set, a desired smooth trajectory is given to the aerial vehicle to compare performance of the proposed controllers in vertical flight mode. This desired trajectory is defined as taking off from initial point $P_0 = [0 \quad 0 \quad 0]^T$, climbing to $P_1 = [4 \quad 4 \quad 5]^T$, tracking a smooth circular

trajectory and landing on center of the circular trajectory $P_2 = [0 \quad 4 \quad 0]^T$, respectively. Desired yaw angle (ψ_d) is set to 0°. In both simulations, 15% parameter estimation error is introduced to the controllers and the aerial vehicle is subjected to external disturbances. These external disturbances are generated as forces and moments produced by wind that is modeled using Dryden Wind-Gust model [70] and they are depicted in Fig. 4.1.
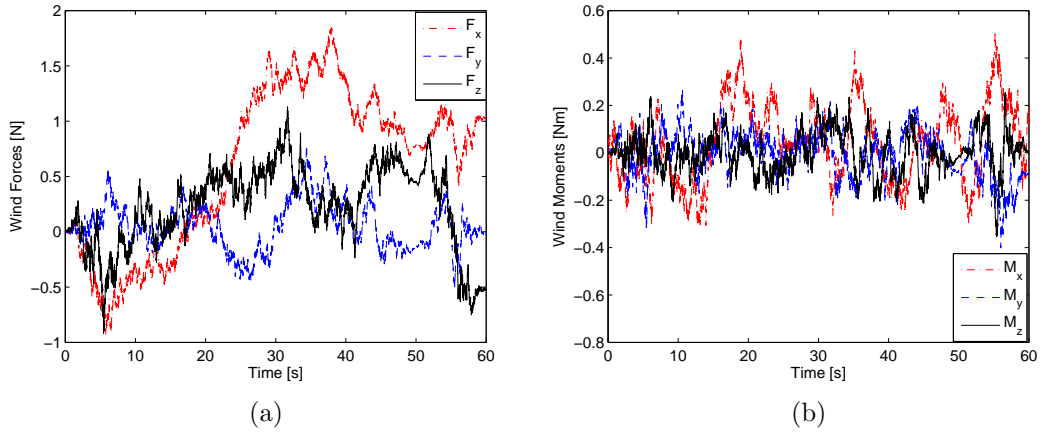
Figure 4.1: External disturbance forces and moments

As can be seen from Fig. 4.2, both control approaches are able to track desired trajectory successfully despite of the external disturbance. Although integral sliding mode controllers lead to slightly smaller position tracking errors, both controllers can keep the position tracking errors in the vicinity of 0.05 m (Fig. 4.3). RMS values of position tracking errors tabulated in Table 4.1 is also demonstrates that position tracking performance of the both controller approaches are comparable. Attitude tracking performance and tracking errors of both control approaches are also depicted in Fig. 4.4 and Fig. 4.5, respectively. Notice that even though both controller approaches are able to keep attitude tracking errors below 0.01 rad, integral sliding mode

controllers can be regarded as more responsive to attitude reference variation. Hence it leads to slightly less error compared to feedback linearization attitude controllers. RMS values of attitude tracking errors are tabulated in Table 4.2.
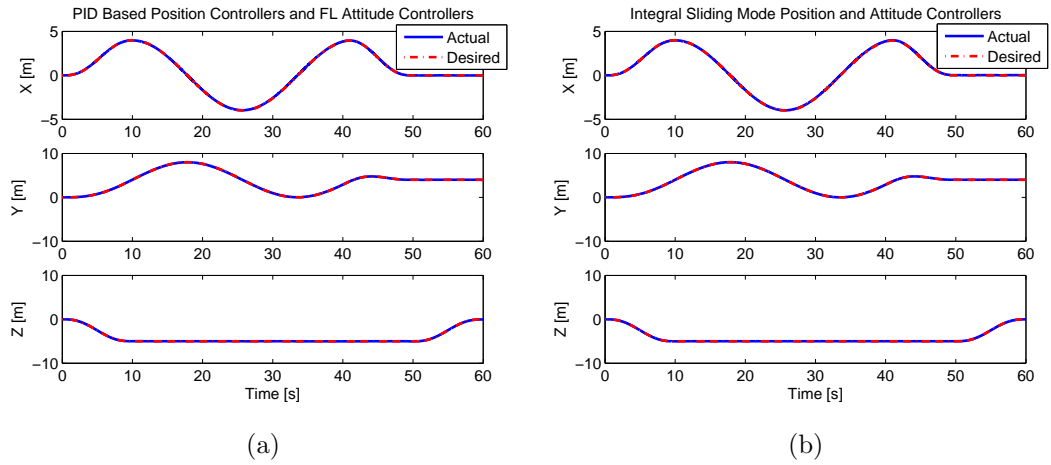
Figure 4.2: Position tracking performance
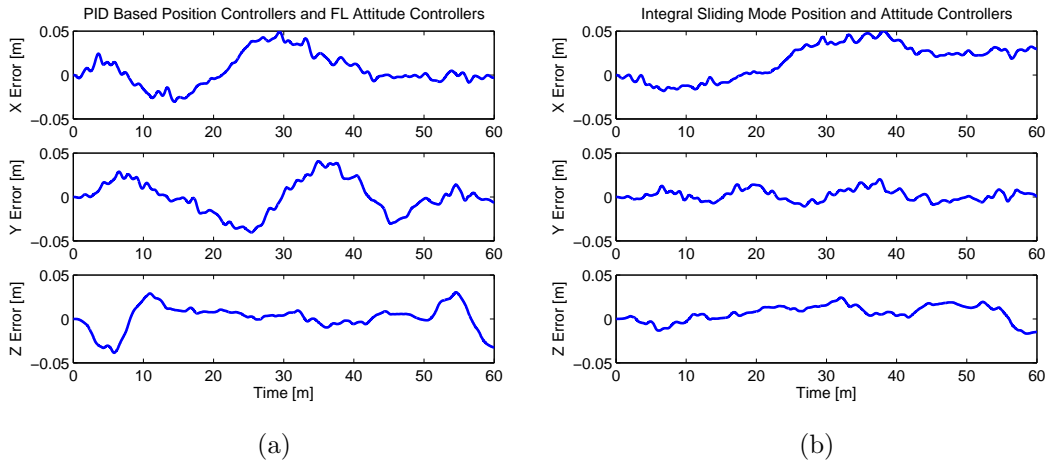
Figure 4.3: Position tracking errors

Table 4.1: Position Tracking RMS Errors

Axis	PID based and FL flight controllers	Integral SMC flight controllers
X	0.0195 m	0.0203 m
Y	0.0195 m	0.0067 m
Z	0.0143 m	0.0115 m

(a) (b)
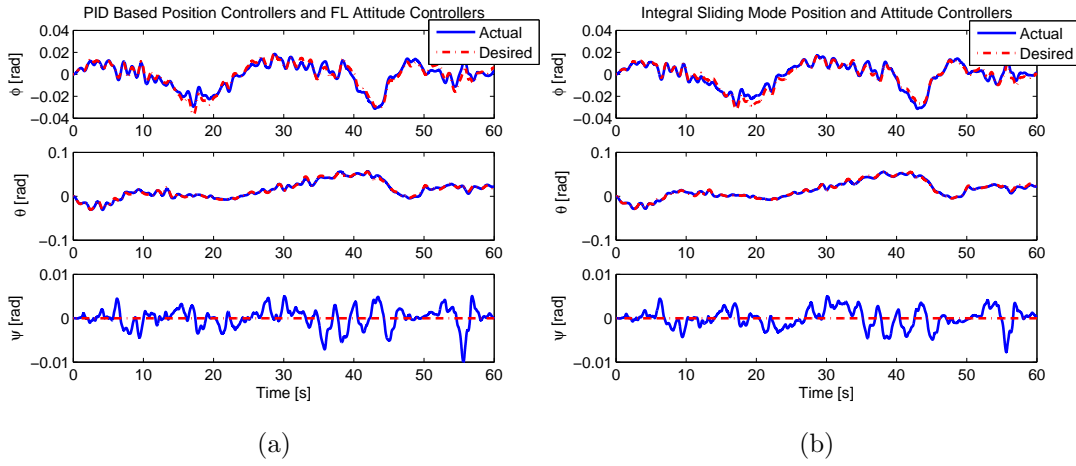
Figure 4.4: Attitude tracking performance

Table 4.2: Attitude Tracking RMS Errors

Axis	PID based and FL flight controllers	Integral SMC flight controllers
ϕ	0.0030 rad	0.0027 rad
θ	0.0020 rad	0.0016 rad
ψ	0.0023 rad	0.0021 rad
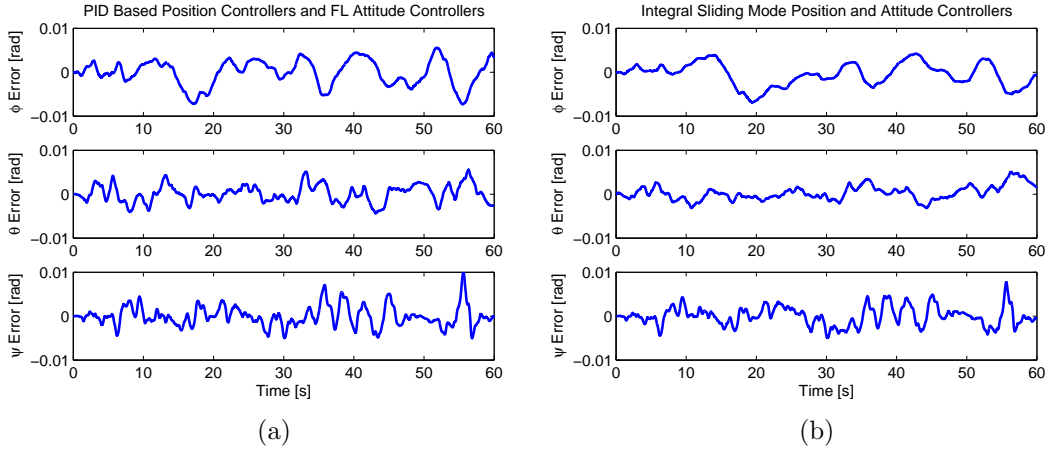
Figure 4.5: Attitude errors

As a result, both flight controllers can track desired smooth circular trajectory under the average external disturbance and give comparable results (Fig. 4.6). Notice that neither of the proposed control approaches exceed the maximum motor thrust limit that is 16 N (Fig. 4.7). They are mostly around the nominal motor thrust which is $45/4 = 11.25N$.
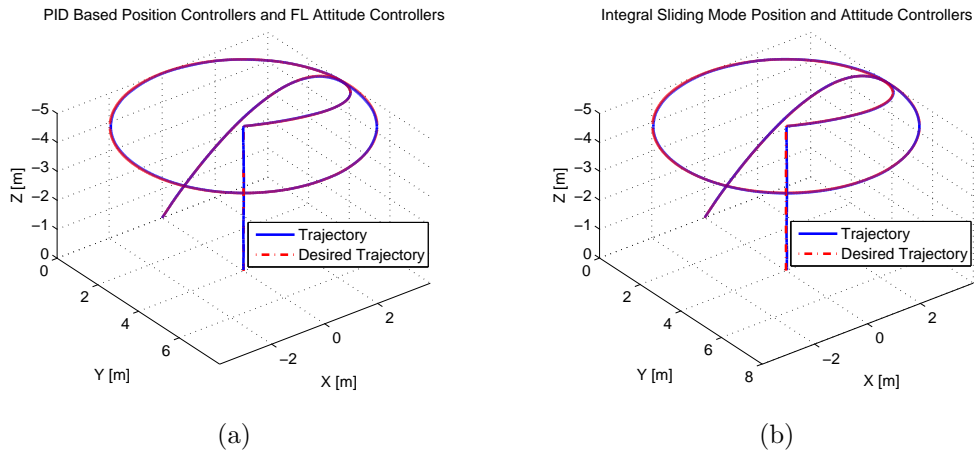
Figure 4.6: Trajectory tracking performance

67
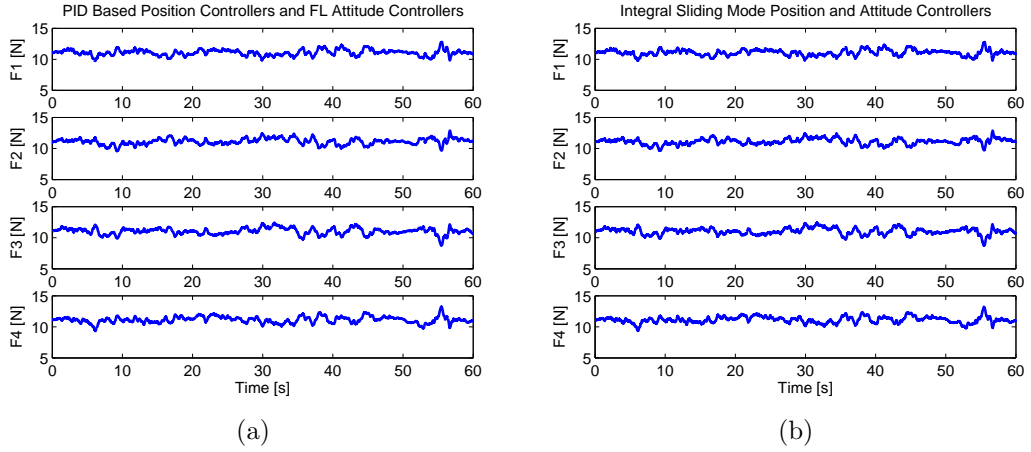
Figure 4.7: Motor thrusts

In the second simulation set, a desired sinusoidal trajectory that includes couple of aggressive maneuvers is given to the aerial vehicle under severe external disturbance. The magnitudes of these external disturbances are almost twice of the disturbance described in the first simulation set (Fig. 4.8). 15% parameter estimation error is also introduced to the controllers. Desired yaw angle (ψ_d) is again set to 0°.
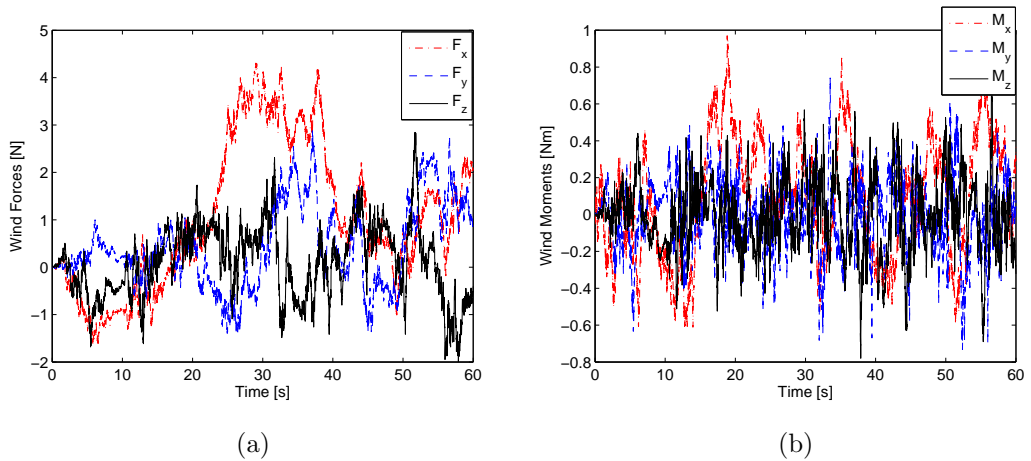
Figure 4.8: External disturbance forces and moments

Position tracking performance and tracking errors of both control approaches are depicted in Fig. 4.9 and Fig. 4.10, respectively. As can be seen from the figures, integral sliding mode flight controllers performs better than PID based approach under the severe disturbance, especially around 30 sec when external disturbance reaches its maximum value.
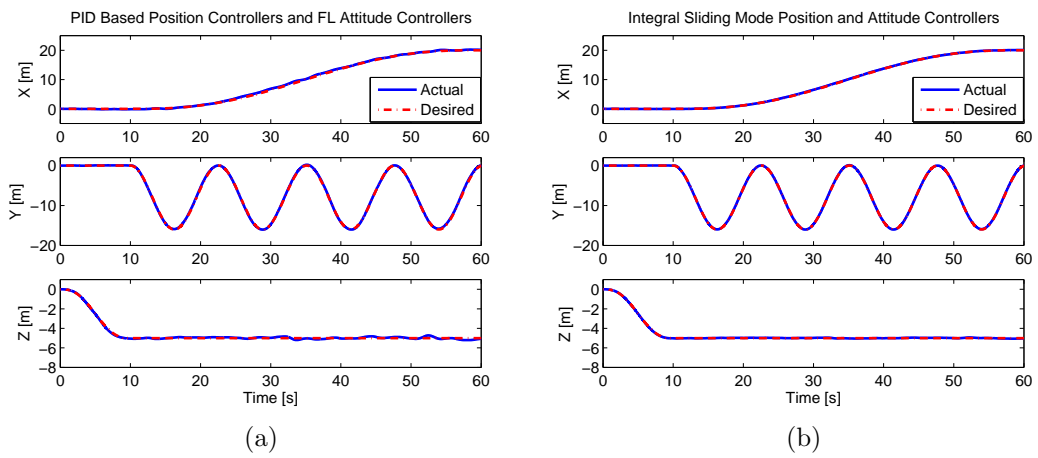
Figure 4.9: Position tracking performance
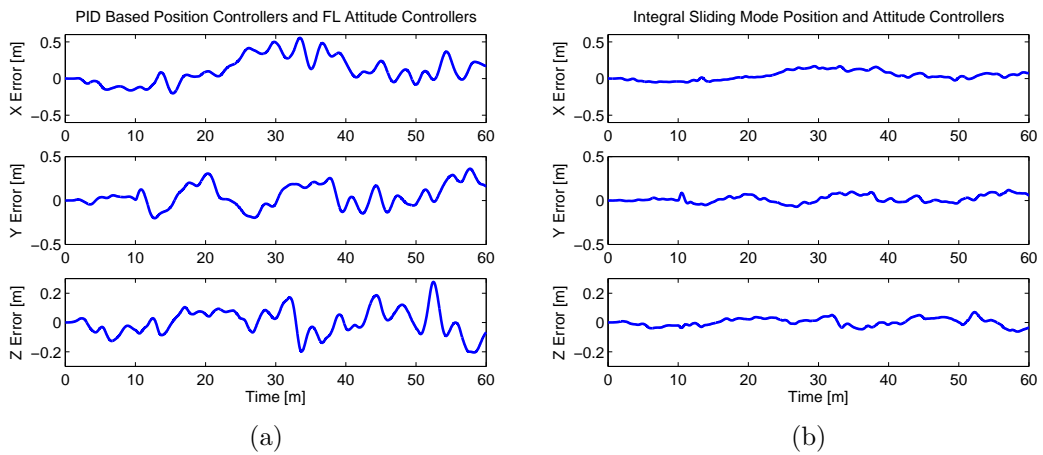
Figure 4.10: Position tracking errors

Moreover, integral sliding mode controllers is able to keep the position tracking errors under 0.1 m, whereas the tracking errors increase up to 0.5 m in PID based approach. This phenomena occurs due to the fact that integral sliding mode controllers have a better disturbance rejection property. Consequently, integral sliding mode controllers also have smaller RMS tracking errors which are tabulated in in Table 4.3.

Table 4.3: Position Tracking RMS Errors

Axis	PID based and FL flight controllers	Integral SMC flight controllers
X	0.2176 m	0.0752 m
Y	0.1424 m	0.0473 m
Z	0.0898 m	0.0275 m

A good position tracking performance stems from the ability of tracing attitude references precisely that is generated by position subsystem. As can be seen from attitude tracking performance and attitude errors depicted in Fig. 4.11 and Fig. 4.12, integral sliding mode flight controllers are more responsive to sudden attitude changes caused by aggressive maneuvering. Notice that integral sliding mode approach is able to keep attitude tracking errors around 0.01 rad, whereas attitude errors made by feedback linearization control approach can rise up to magnitude of 0.05 rad. For comparison purpose RMS values of attitude tracking errors are also tabulated in Table 4.4.
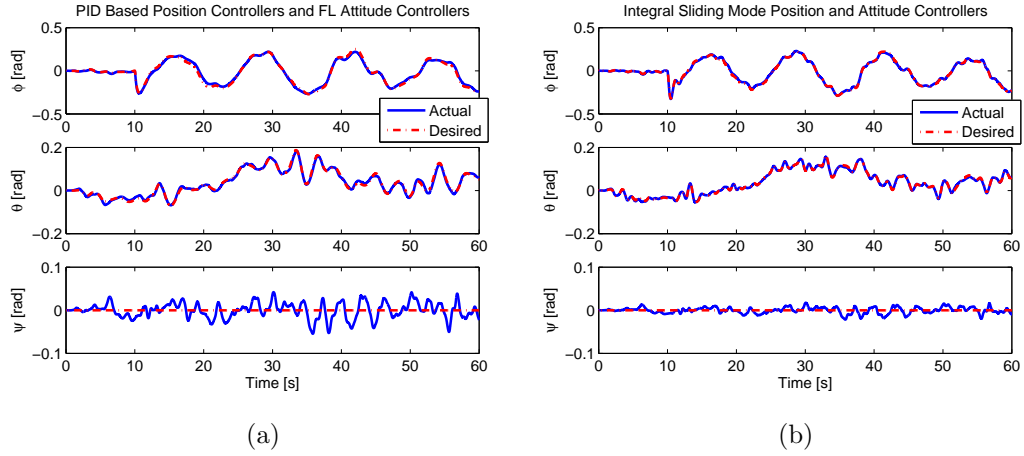
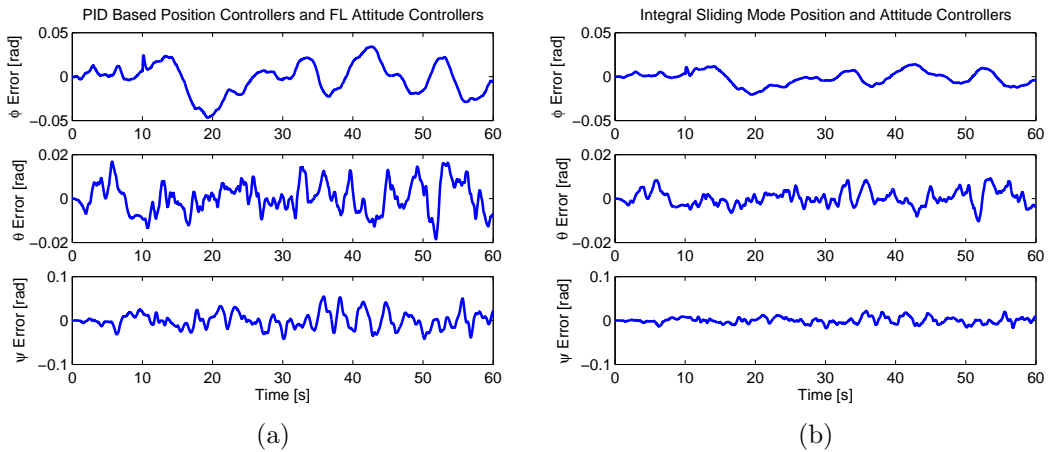Figure 4.11: Attitude tracking performance

Figure 4.12: Attitude errors

The trajectory tracking performance of the both control approaches are given in Fig. 4.13. It can clearly be seen that PID based position and feedback linearization attitude controllers fail to track desired trajectory where sudden maneuvers is required. On the other hand, integral sliding mode flight controllers can smoothly achieve to perform sudden maneuvers.

71

Table 4.4: Attitude Tracking RMS Errors

Axis	PID based and FL flight controllers	Integral SMC flight controllers
ϕ	0.0181 rad	0.0080 rad
θ	0.0069 rad	0.0035 rad
ψ	0.0182 rad	0.0071 rad

Notice that both control approaches generate extra motor thrusts, that is in the vicinity of maximum value, to resist severe external disturbance and to realize aggressive maneuvers (Fig. 4.14).

(a)   (b)
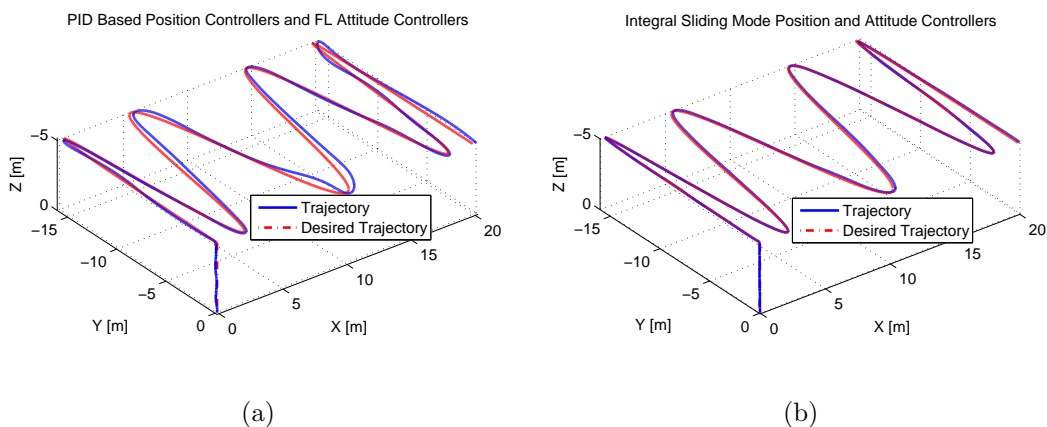
Figure 4.13: Trajectory tracking performance

To conclude, the two simulation sets demonstrate that both control approaches lead to comparably successful results when the smooth trajectory is required to be tracked under normal external disturbance. However, integral sliding mode flight controllers performs better than PID based position and feedback linearization attitude controllers, if the aerial vehicle is subjected to severe external disturbance and the aerial vehicle is required to realize

aggressive maneuvers that enforce the motor thrusts to the limits.
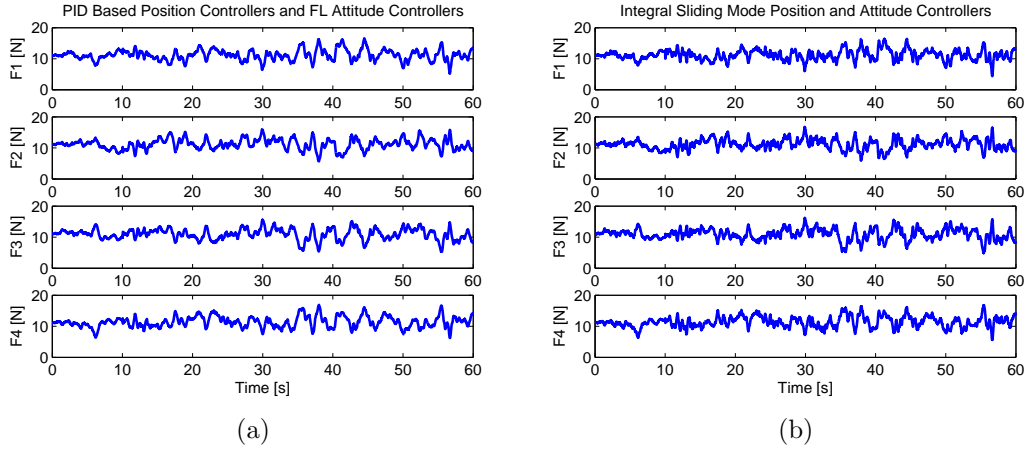
Figure 4.14: Motor thrusts

4.1.2 A Full Flight Scenario

In this section, a typical surveillance scenario is considered which covers vertical, transition and horizontal flight modes of the aerial vehicle. For the vertical mode position control, PID based position controllers are employed, whereas feedback linearization attitude controllers are used for the attitude subsystem. As for the transition and horizontal flight modes, transition and horizontal mode position controllers together with feedback linearization attitude controllers are employed. The surveillance scenario is described as follows: during the first 10 sec, the aerial vehicle takes off and climbs to 10 m in vertical mode ($\theta_f = \theta_r = 90°$). Then it begins to tilt its wings between 10-20 sec, while it is moving in X direction and preserving its altitude. After wings reach 17° angle of attack in transition mode, the aerial vehicle flies to the desired location in horizontal mode with constant 17° wing angle between 20-50 sec. Then, the aerial vehicle tilts its wings back to 90° in

73

transition mode (50-60 sec) and then tracks a circular trajectory in vertical mode (60-90 sec). Finally it lands in 20 sec in vertical mode. Throughout the flight, desired yaw is set to 0°. In order to test performance of the developed controllers, external disturbances are also included. These external disturbances are generated as forces and moments produced by wind that is modeled using Dryden Wind-Gust model and depicted in Figure 4.15.
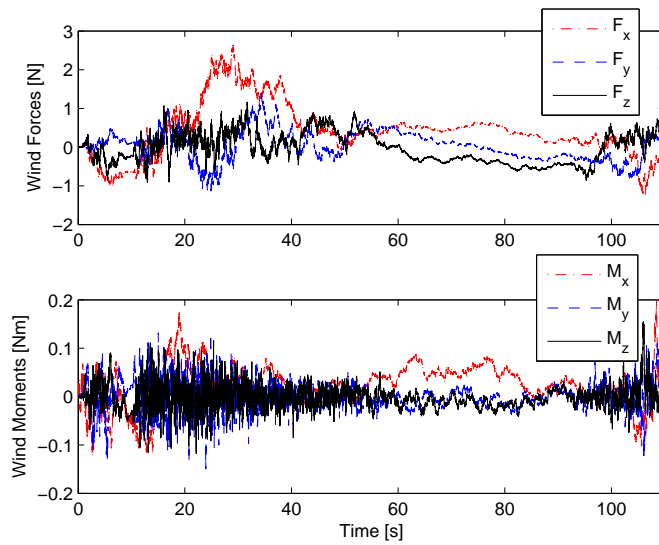

Figure 4.15: Wind forces and moments

Position and attitude tracking performance are depicted in Figures 4.16 and 4.17, respectively. Note that altitudes take negative values, since the Z axis in the world frame is directed downwards. As can be seen from the figures, the aerial vehicle successfully tracks the desired trajectory. During transition and horizontal flight (10-60 sec), pitch angle is set to 0° and roll angle is changing frequently to counteract wind forces and moments. On the other hand, the aerial vehicle continuously changes its attitude to track desired trajectory in vertical mode (60-110 sec).
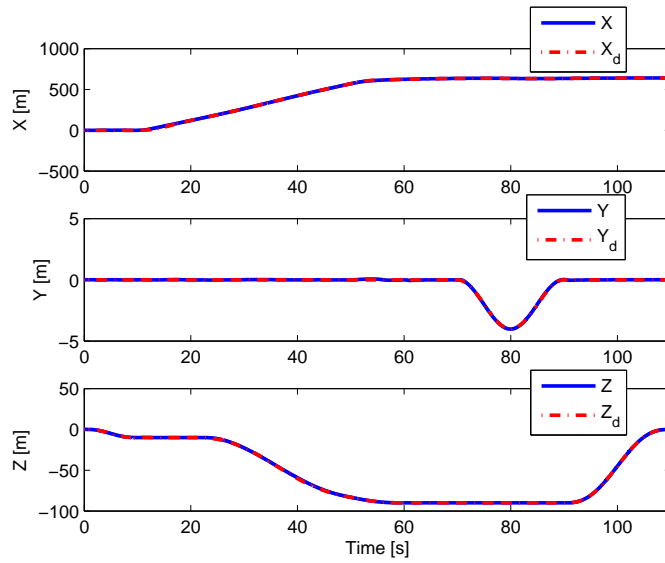
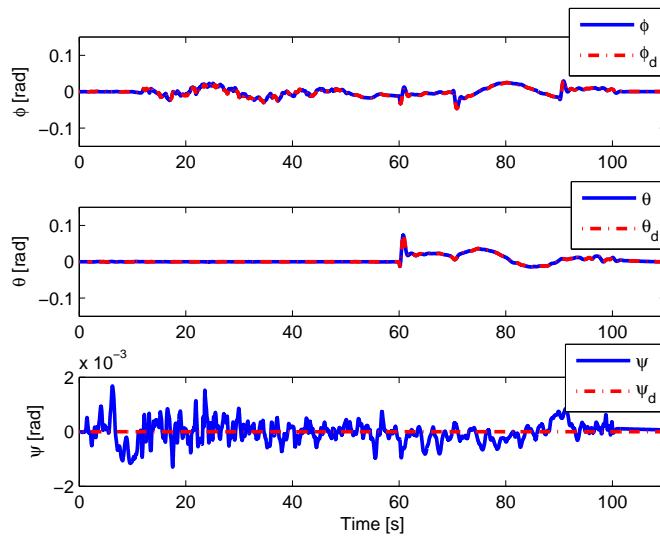Figure 4.16: Position tracking performance

Figure 4.17: Attitude tracking performance

Figure 4.18 demonstrates trajectory tracking performance throughout the flight and Figure 4.19 shows trajectory tracking and landing performance in

75

vertical mode. After successful horizontal flight the aerial vehicle tracks circular trajectory and lands on the desired position ($[640, 0, 0]$) in vertical mode.
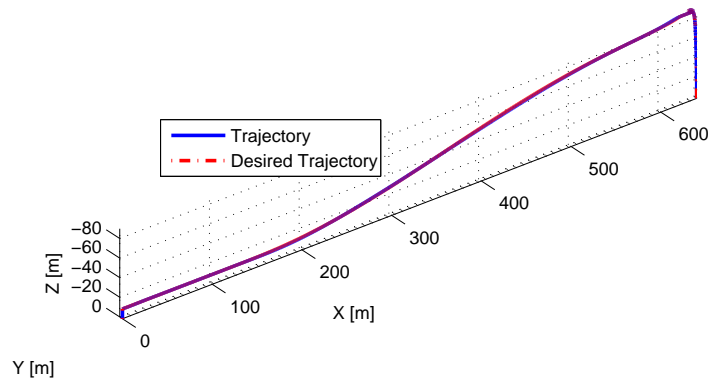

Figure 4.18: Trajectory tracking

Figure 4.20 depicts motor thrusts produced by rotors. Notice that in vertical mode, each motor produces approximately 11.25 N to compensate the aerial vehicle's weight. Due to tilted motors and wings, vertical component of the total thrust decreases in transition mode (10-20 and 50-60 sec). Hence, in order to counteract aerial vehicle's weight higher motor thrusts are needed. As can be seen from the figure motor thrusts increase without exceeding maximum capacity of motors, 16 N, in transition mode. On the other hand, motor thrusts are reduced to their 20% due to the lift forces (Fig. 4.21) generated by wings in horizontal mode (20-50 sec). Since the aerial vehicle consumes less power and saves energy, the flight endurance increases and the vehicle flies longer with the same battery capacity.
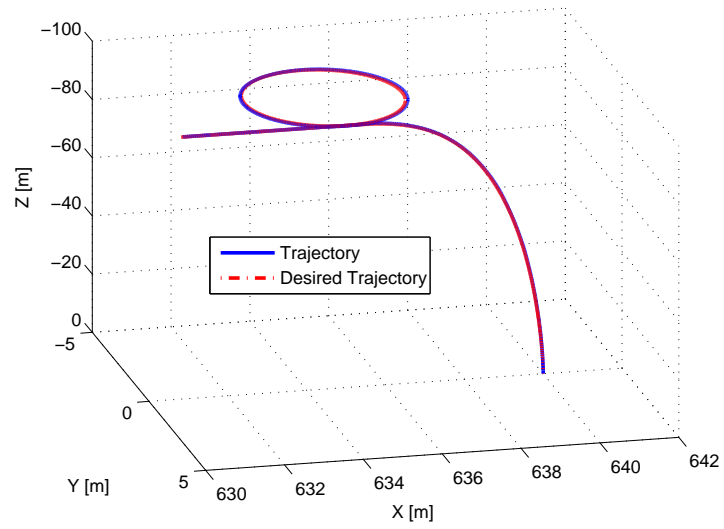
76

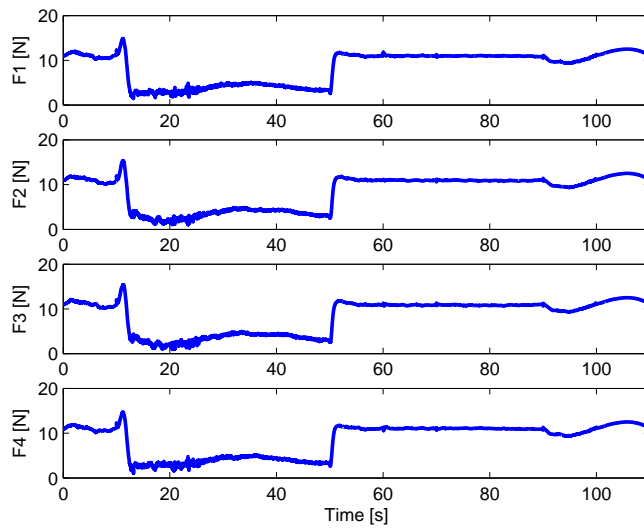Figure 4.19: Trajectory tracking and landing in the vertical mode
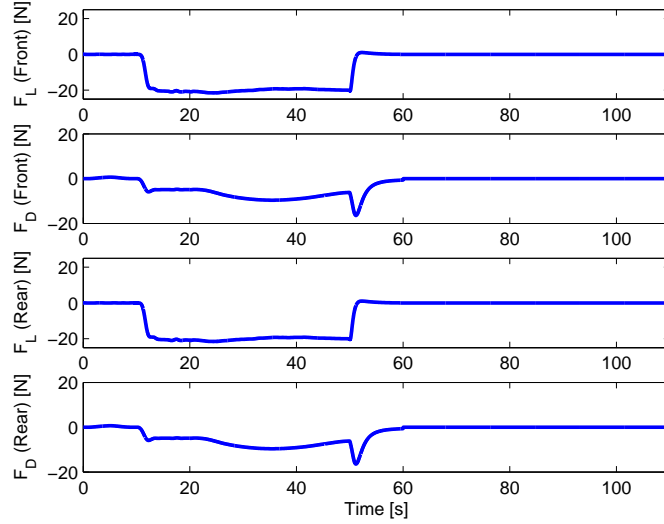

Figure 4.20: Motor thrusts

Figure 4.21: Aerodynamic forces

4.2 Experimental Results

The proposed flight controller architecture is also tested in real flight experiments. In this tests, for the vertical flight mode of the aerial vehicle PID based vertical mode position controllers and feedback linearization attitude controllers are implemented due to the fact that their ease of implementation and satisfactory performance under average weather conditions. Transition and horizontal mode position controllers together with feedback linearization attitude controllers are also implemented for the transition and horizontal flight modes.

First, vertical flight tests are performed in helicopter field of Sabanci University campus under average wind and gust conditions. Snapshots from this vertical flight test are depicted Fig. 4.22, whereas attitude and the altitude flight data are given in Fig. 4.23.

Figure 4.22: Vertical fligt test with SUAVI in university campus

Despite the existence of large vertical surfaces (wings) in the vertical flight mode, performance of the air vehicle is found to be stable and promising. The roll, pitch and heading angles do not exceed the reference angles for more than 4° during the flight and the deviation of the altitude is bounded by a total of 25 cm. The aircraft is drifted by the winds due to its vertical wings, which act like sails in hover, but it can recover itself to its initial position and land safely.
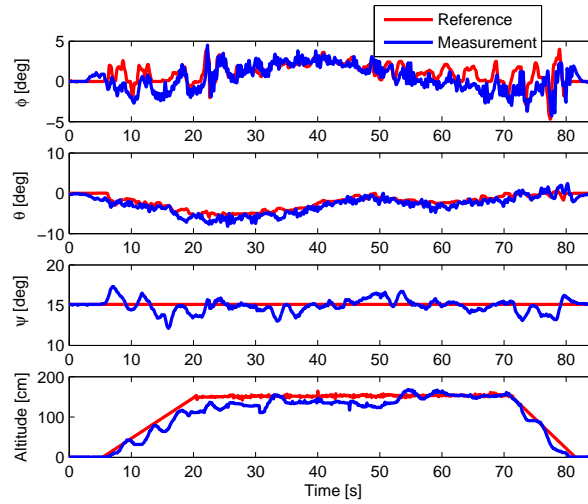

Figure 4.23: Vertical flight data

After the successful vertical flight tests with good stabilization performance, a full flight test which includes vertical, transition and horizontal flight modes of the aerial vehicle is also carried out. In these tests, SUAVI takes off vertically until reaching a reference altitude and then tilted the wings gradually to the angle of attacks of the desired forward speed. During these tests, flights with up to 40 km/h horizontal speed are accomplished and SUAVI is landed safely. Snapshots from the flight test and desired trajectory of the aerial vehicle are presented in Fig. 4.25 and Fig. 4.26, respectively.

80

Figure 4.24: Full flight test snapshots

Figure 4.25: Desired trajectory

Attitude and altitude references and measurements that are obtained in this test are also depicted in Fig. 4.27. It is seen in the figures that the roll reference was changed for the tracking of position reference, whereas the pitch reference is kept at 0° during the horizontal flight. It is also observed that the errors in roll, pitch and heading reference tracking were bounded by 5°, which is quite reasonable in the existence of gusts, and altitude reference tracking was quite satisfactory. Note that the measured position tracking is curved (Fig. 4.27) due to the cross wind during the flight.
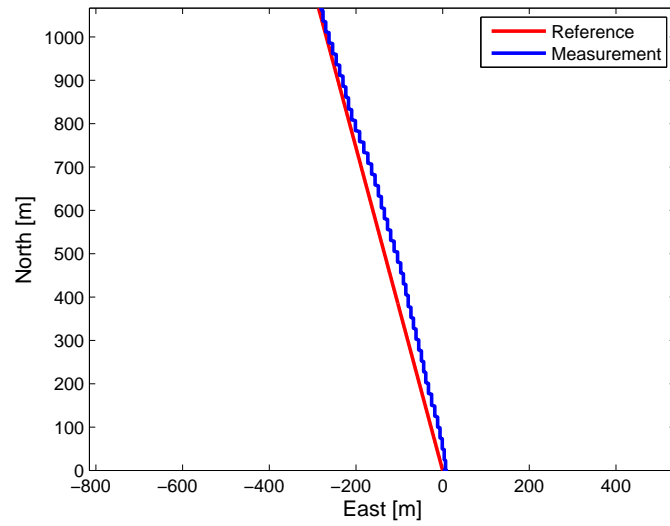
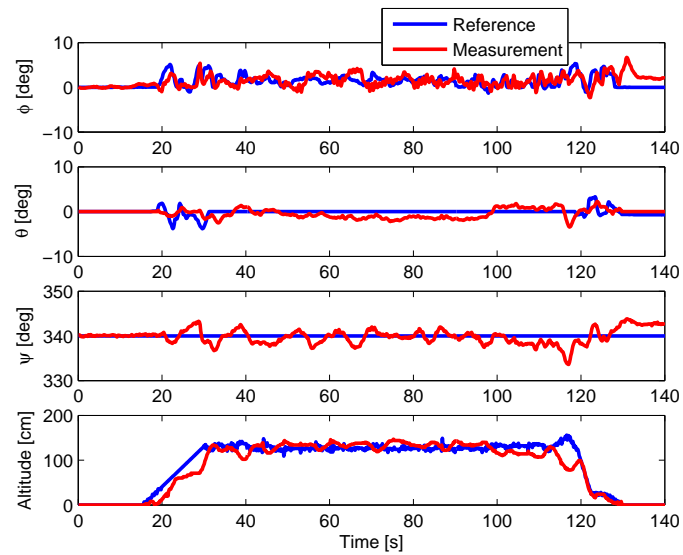Figure 4.26: Full flight test GPS position data

Figure 4.27: Full flight test attitude and altitude data

Chapter V

5   Concluding Remarks and Future Works

In this thesis, A full nonlinear dynamical model including explicit mathematical models for various flight modes and attitude dynamics expressed in world frame without hover assumption is derived using Newton-Euler method. In dynamical modeling, actuation vector is simplified to design flight controllers.

A hierarchical control system architecture, including a high level controller and low-level controllers, is designed and implemented. In line with the control system hierarchy, vertical, transition and horizontal mode flight controllers are developed. In order to design flight controllers, the dynamics of the aerial vehicle is divided into two subsystems, namely position and attitude subsystems. Several position controllers are designed for position subsystem that has slower dynamics when compared with the attitude subsystem. Reference attitude angles are computed by utilizing the dynamic inversion method and they are used by the attitude controllers that are designed for attitude subsystem.

For vertical flight mode of the aerial vehicle, integral sliding mode and PID based position controllers via dynamic inversion method are proposed, whereas feedback linearization and integral sliding mode attitude controllers are designed for attitude subsystem in all three flight modes of SUAVI. Ver-

tical flight simulations demonstrate that both control approaches lead to comparably successful results when the smooth trajectory is required to be tracked under the average external disturbance. However, integral sliding mode flight controllers performs better than PID based position and feedback linearization attitude controllers, if the aerial vehicle is subjected to severe external disturbance and the aerial vehicle is required to realize aggressive maneuvers. Moreover, full flight simulation that covers various flight modes of the aerial is carried out and results demonstrate that the performance of the proposed control approaches is successful and promising.

The proposed PID based vertical mode position controllers, transition and horizontal mode position controllers together with feedback linearization attitude controllers is also tested in real flight experiments. Results of several flight test that are carried out in Sabanci University campus and on a wide road outside the campus demonstrate successful performance of proposed control architecture.

Future works include implementation of integral sliding mode flight controllers on the aerial vehicle and performing aggressive maneuvers in real flight test.

Appendix A

Velocity Transformation Matrix

According to a right-hand coordinate system, the three rotations are described by

- Rotation about x-axis by ϕ, R_x

$$R_x = \begin{bmatrix} 1 & 0 & 0 \\ 0 & c_\phi & -s_\phi \\ 0 & s_\phi & c_\phi \end{bmatrix} \tag{A-1}$$

- Rotation about y-axis by θ, R_y

$$R_y = \begin{bmatrix} c_\theta & 0 & s_\theta \\ 0 & 1 & 0 \\ -s_\theta & 0 & c_\theta \end{bmatrix} \tag{A-2}$$

- Rotation about z-axis by ψ, R_z

$$R_z = \begin{bmatrix} c_\psi & -s_\psi & 0 \\ s_\psi & c_\psi & 0 \\ 0 & 0 & 1 \end{bmatrix} \tag{A-3}$$

The velocity transformation matrix $\mathbb{E}$ can be obtained by resolving the time derivative of the attitude angles into the body-fixed frame as shown below

$$
\begin{bmatrix} p \\ q \\ r \end{bmatrix} = \begin{bmatrix} \dot{\phi} \\ 0 \\ 0 \end{bmatrix} + R_x{}^T \begin{bmatrix} 0 \\ \dot{\theta} \\ 0 \end{bmatrix} + R_x{}^T R_y{}^T \begin{bmatrix} 0 \\ 0 \\ \dot{\psi} \end{bmatrix}
$$

$$
\Rightarrow \begin{bmatrix} \dot{\phi} \\ 0 \\ 0 \end{bmatrix} + \begin{bmatrix} 1 & 0 & 0 \\ 0 & c_\phi & s_\phi \\ 0 & -s_\phi & c_\phi \end{bmatrix} \begin{bmatrix} 0 \\ \dot{\theta} \\ 0 \end{bmatrix} + \begin{bmatrix} 1 & 0 & 0 \\ 0 & c_\phi & s_\phi \\ 0 & -s_\phi & c_\phi \end{bmatrix} \begin{bmatrix} c_\theta & 0 & -s_\theta \\ 0 & 1 & 0 \\ s_\theta & 0 & c_\theta \end{bmatrix} \begin{bmatrix} 0 \\ 0 \\ \dot{\psi} \end{bmatrix}
$$

$$
\Rightarrow \begin{bmatrix} \dot{\phi} \\ 0 \\ 0 \end{bmatrix} + \begin{bmatrix} 0 \\ c_\phi \dot{\theta} \\ -s_\phi \dot{\theta} \end{bmatrix} + \begin{bmatrix} c_\theta & 0 & -s_\theta \\ s_\phi s_\theta & c_\phi & s_\phi c_\theta \\ c_\phi s_\theta & -s_\phi & c_\phi c_\theta \end{bmatrix} \begin{bmatrix} 0 \\ 0 \\ \dot{\psi} \end{bmatrix}
$$

$$
\Rightarrow \begin{bmatrix} \dot{\phi} \\ 0 \\ 0 \end{bmatrix} + \begin{bmatrix} 0 \\ c_\phi \dot{\theta} \\ -s_\phi \dot{\theta} \end{bmatrix} + \begin{bmatrix} -s_\theta \dot{\psi} \\ s_\phi c_\theta \dot{\psi} \\ c_\phi c_\theta \dot{\psi} \end{bmatrix}
$$

$$
\Rightarrow \begin{bmatrix} \dot{\phi} - s_\theta \dot{\psi} \\ c_\phi \dot{\theta} + s_\phi c_\theta \dot{\psi} \\ -s_\phi \dot{\theta} + c_\phi c_\theta \dot{\psi} \end{bmatrix} = \begin{bmatrix} 1 & 0 & -s_\theta \\ 0 & c_\phi & s_\phi c_\theta \\ 0 & -s_\phi & c_\phi c_\theta \end{bmatrix} \begin{bmatrix} \dot{\phi} \\ \dot{\theta} \\ \dot{\psi} \end{bmatrix} \triangleq \mathbb{E} \begin{bmatrix} \dot{\phi} \\ \dot{\theta} \\ \dot{\psi} \end{bmatrix} \qquad (A\text{-}4)
$$

Appendix B

Derivation of $\dot{\mathbb{E}} = -\mathbb{E}\dot{\mathbb{B}}\mathbb{E}$

Recall that velocity transformation matrix $\mathbb{E}$ is the inverse of the matrix $\mathbb{B}$; i.e.

$$\mathbb{E}\mathbb{B} = I \tag{B-1}$$

where I is 3×3 identity matrix. By taking derivative of both sides of Eqn. (B-1), we have

$$\dot{\mathbb{E}}\mathbb{B} + \mathbb{E}\dot{\mathbb{B}} = 0$$

$$\Rightarrow \dot{\mathbb{E}}\mathbb{B} = -\mathbb{E}\dot{\mathbb{B}} \tag{B-2}$$

Multiplying both sides of Eqn. (B-2) by $\mathbb{E}$ from the right and using Eqn. (B-1), the following equality can be obtained:

$$\dot{\mathbb{E}}\underbrace{\mathbb{B}\mathbb{E}}_{I} = \mathbb{E}\dot{\mathbb{B}}\mathbb{E}$$

$$\Rightarrow \dot{\mathbb{E}} = -\mathbb{E}\dot{\mathbb{B}}\mathbb{E} \tag{B-3}$$

Appendix C

Derivation of Dynamic Inversion Formulas

From Chapter 3, first recall that

$$\tilde{\mu}_1 = (c_{\psi_d} c_{\theta_d} c_{\theta_f} - (c_{\phi_d} s_{\theta_d} c_{\psi_d} + s_{\phi_d} s_{\psi_d}) s_{\theta_f}) u_1 \tag{C-1}$$

$$\tilde{\mu}_2 = (s_{\psi_d} c_{\theta_d} c_{\theta_f} - (c_{\phi_d} s_{\theta_d} s_{\psi_d} - s_{\phi_d} c_{\psi_d}) s_{\theta_f}) u_1 \tag{C-2}$$

$$\tilde{\mu}_3 = (-s_{\theta_d} c_{\theta_f} - c_{\phi_d} c_{\theta_d} s_{\theta_f}) u_1 \tag{C-3}$$

By defining horizontal and vertical component of the total thrust as

$$P \triangleq u_1 c_{\theta_f} \tag{C-4}$$

$$Q \triangleq u_1 s_{\theta_f} \tag{C-5}$$

Equations (C-1)-(C-3) become

$$\tilde{\mu}_1 = c_{\psi_d} c_{\theta_d} P - (c_{\phi_d} s_{\theta_d} c_{\psi_d} + s_{\phi_d} s_{\psi_d}) Q \tag{C-6}$$

$$\tilde{\mu}_2 = s_{\psi_d} c_{\theta_d} P - (c_{\phi_d} s_{\theta_d} s_{\psi_d} - s_{\phi_d} c_{\psi_d}) Q \tag{C-7}$$

$$\tilde{\mu}_3 = -s_{\theta_d} P - c_{\phi_d} c_{\theta_d} Q \tag{C-8}$$

By multiplying both sides of the Eqns. (C-6) and (C-7) with c_{ψ_d} and s_{ψ_d}, respectively, and adding them up, we obtain

$$c_{\theta_d} P - c_{\phi_d} s_{\theta_d} Q = \tilde{\mu}_1 c_{\psi_d} + \tilde{\mu}_2 s_{\psi_d} \tag{C-9}$$

Then multiply equation (C-9) by c_{θ_d} and equation (C-8) by $-s_{\theta_d}$, and sum the resultant equations up, we have

$$P = (\tilde{\mu}_1 c_{\psi_d} + \tilde{\mu}_2 s_{\psi_d})c_{\theta_d} - \tilde{\mu}_3 s_{\theta_d} \tag{C-10}$$

Again multiply equation (C-9) by s_{θ_d} and equation (C-8) by c_{θ_d}, and add the resultant equations up, we obtain

$$-c_{\phi_d}Q = (\tilde{\mu}_1 c_{\psi_d} + \tilde{\mu}_2 s_{\psi_d})s_{\theta_d} + \tilde{\mu}_3 c_{\theta_d} \tag{C-11}$$

Lastly, multiplying both sides of the Eqns. (C-6) and (C-7) with s_{ψ_d} and $-c_{\psi_d}$, respectively, and adding them up, we have

$$s_{\phi_d}Q = \tilde{\mu}_1 s_{\psi_d} - \tilde{\mu}_2 c_{\psi_d} \tag{C-12}$$

By defining auxiliary variables γ_1 and γ_2 as

$$\gamma_1 \triangleq \tilde{\mu}_1 \cdot c_{\psi_d} + \tilde{\mu}_2 \cdot s_{\psi_d} \tag{C-13}$$

$$\gamma_2 \triangleq \tilde{\mu}_1 \cdot s_{\psi_d} - \tilde{\mu}_2 \cdot c_{\psi_d} \tag{C-14}$$

Equations (C-10)-(C-12) become

$$P = \gamma_1 c_{\theta_d} - \tilde{\mu}_3 s_{\theta_d} \tag{C-15}$$

$$-c_{\phi_d}Q = \gamma_1 s_{\theta_d} + \tilde{\mu}_3 c_{\theta_d} \tag{C-16}$$

$$s_{\phi_d}Q = \gamma_2 \tag{C-17}$$

By taking square of Eqns. (C-15)-(C-17), and summing the resultant equations up, we obtain the following equation

$$P^2 + Q^2 {c_{\phi_d}}^2 + Q^2 {s_{\phi_d}}^2 =$$

$${\gamma_1}^2 {c_{\theta_d}}^2 - 2\gamma_1 \tilde{\mu}_3 c_{\theta_d} s_{\theta_d} + \tilde{\mu}_3^2 {s_{\theta_d}}^2 + {\gamma_1}^2 {s_{\theta_d}}^2 + 2\gamma_1 \tilde{\mu}_3 c_{\theta_d} s_{\theta_d} + \tilde{\mu}_3^2 {c_{\theta_d}}^2 + {\gamma_2}^2$$

$$\Rightarrow P^2 + Q^2 ({c_{\phi_d}}^2 + {s_{\phi_d}}^2) = {\gamma_1}^2 ({c_{\theta_d}}^2 + {s_{\theta_d}}^2) + {\gamma_2}^2 + \tilde{\mu}_3^2 ({c_{\theta_d}}^2 + {s_{\theta_d}}^2)$$

$$\Rightarrow P^2 + Q^2 = {\gamma_1}^2 + {\gamma_2}^2 + \tilde{\mu}_3^2 \qquad \text{(C-18)}$$

By substituting Eqns. (C-4), (C-5), (C-13) and (C-14) into Eqn. (C-18); and taking square root of the both side of the resultant equation, we obtain following equality for the total thrust

$$u_1^2 {s_{\phi_d}}^2 + u_1^2 {c_{\phi_d}}^2 = \tilde{\mu}_1^2 {c_{\psi_d}}^2 + 2\tilde{\mu}_1\tilde{\mu}_2 c_{\psi_d} s_{\psi_d} + \tilde{\mu}_2^2 {s_{\psi_d}}^2 + \tilde{\mu}_1^2 {s_{\psi_d}}^2 - 2\tilde{\mu}_1\tilde{\mu}_2 c_{\psi_d} s_{\psi_d} + \tilde{\mu}_2^2 {c_{\psi_d}}^2 + \tilde{\mu}_3^2$$

$$\Rightarrow u_1^2 ({s_{\phi_d}}^2 + {c_{\phi_d}}^2) = \tilde{\mu}_1^2 ({c_{\psi_d}}^2 + {s_{\psi_d}}^2) + \tilde{\mu}_2^2 ({c_{\psi_d}}^2 + {s_{\psi_d}}^2) + \tilde{\mu}_3^2$$

$$\Rightarrow u_1^2 = \tilde{\mu}_1^2 + \tilde{\mu}_2^2 + \tilde{\mu}_3^2$$

$$\Rightarrow u_1 = \sqrt{\tilde{\mu}_1^2 + \tilde{\mu}_2^2 + \tilde{\mu}_3^2} \qquad \text{(C-19)}$$

With known u_1, desired roll angle (ϕ_d) can easily be computed from Eqns. (C-17) and (C-5) as

$$s_{\phi_d} u_1 s_{\theta_f} = \gamma_2$$

$$\Rightarrow \phi_d = \arcsin\left(\frac{\gamma_2}{u_1 \cdot s_{\theta_f}}\right) \qquad \text{(C-20)}$$

In order to find desired pitch angle (θ_d), one can multiply Eqn. (C-15) by $-\tilde{\mu}_1$ and Eqn. (C-16) by γ_1, and add the resultant equations up as follows

$$-\tilde{\mu}_3\gamma_1 c_{\theta_d} + \tilde{\mu}_3^2 s_{\theta_d} + \tilde{\mu}_3\gamma_1 c_{\theta_d} + \gamma_1{}^2 s_{\theta_d} = -\tilde{\mu}_3 P - \gamma_1 c_{\phi_d} Q$$

$$\Rightarrow (\tilde{\mu}_3^2 + \gamma_1{}^2) s_{\theta_d} = -\tilde{\mu}_3 P - \gamma_1 c_{\phi_d} Q \tag{C-21}$$

By substituting Eqns. (C-4) and (C-5) into Eqn. (C-21); and using known ϕ_d and u_1, desired pitch angle can be computed as

$$\theta_d = \arcsin\left(\frac{-\tilde{\mu}_3 \cdot u_1 \cdot c_{\theta_f} - u_1 \cdot \gamma_1 \cdot s_{\theta_f} \cdot c_{\phi_d}}{\gamma_1{}^2 + \tilde{\mu}_3^2}\right) \tag{C-22}$$

92

References

[1] Office of the Secretary of Defense. Unmanned Aerial Vehicles Roadmap 2005-2030, 2002.

[2] H. Eisenbeiss. A mini Unmanned Aerial Vehicle (UAV): System overview and image acquisition. *International Workshop on "Processing and Visualization Using High-Resolution Imagery*, 2004.

[3] M. Aehmet Ali Erbil, S. D. Prior, M. Karamanoglu, Barlow Odedra, S., C., and D. Lewis. Reconfigurable Unmanned Aerial Vehicles. In *International Conference on Manufacturing and Engineering Systems*, pages 392–396, 2009.

[4] Z. Sarris. Survey of UAV applicaitons in Civil Market. 2001.

[5] Henri Eisenbeis. UAV Photogrammetry. Master's thesis, ETH Zurich, 2009.

[6] C. H. Gibbs-Smith. *An Historical Survey from its Origins to the end of World War II.* The Science Museum, 1970.

[7] C. H. Gibbs-Smith. *The Aeroplane: An Historical Survey of its Origins and Development.* The Science Museum, 1960.

[8] D. J. Fratello T. H. Cox, I. Somers. Earth observations and the role of UAVs: a capabilities assessment. *Courier Dover Publications*, 1.1:9–11, 2006.

[9] BQM-34 Firebee 3-View, July 2011. [online] `http://www.fas.org/irp/program/collect/Firebee-Sys-Desc.pdf`.

[10] T. P. Ehrhard. *Air Force UAVs: The Secret History.* Mitchell Institute Press, July 2010.

[11] Proteus, June 2011. [online] `http://www.nasa.gov/centers/dryden/news/FactSheets/FS-069-DFRC.html`.

[12] K. Nonami. Prospect and Recent Research & Development for Civil Use Autonomous Unmanned Aircraft as UAV and MAV. *Journal of System Design and Dynamics*, 1(2):120–128, 2007.

[13] Heron, June 2011. [online] `http://www.iai.co.il/18900-16382-en/BusinessAreas_UnmannedAirSystems_HeronFamily.aspx`.

[14] Fire Scout VTUAV Unmanned Aerial Vehicle, June 2011. [online] `http://www.naval-technology.com/projects/firescout/`.

[15] I. Somers T. H. Cox, C. J. Nagy. Civil UAV Capability Assessment, December 2004.

[16] R. Finkelstein. The Ubiquitous UAV, 2009. [online] `http://www.robotictechnologyinc.com/images/upload/file/The_Ubiquitous_UAV.pdf`.

[17] U.S Army Unmanned Aircraft Systems Roadmap 2010-2035, 2010.

[18] M. D. F. Bento. Unmanned Aerial Vehicles: An Overwiev. *Insede GNSS Magazine*, pages 54–62, February 2008.

[19] FanCopter, June 2011. [online] `http://www.emt-penzberg.de/index.php?10&L=1`.

[20] Raven, June 2011. [online] `http://www.avinc.com/glossary/raven`.

[21] Hermes 1500, June 2011. [online] `http://www.elbitsystems.com/elbitmain/area-in2.asp?parent=3&num=30&num2=30`.

[22] RQ 15 Neptune, June 2011. [online] `http://www.drs-ds.com/Products/UAS/neptune.aspx`.

[23] RQ-4 Global Hawk High-Altitude, Long-Endurance Unmanned Aerial Reconnaissance System, July 2011. [online] `http://www.as.northropgrumman.com/products/ghrq4b/assets/HALE_Factsheet.pdf`.

[24] Investigation of the Helios Prototype Aircraft - Mishap Volume I Mishap Report, July 2011. [online] `http://www.nasa.gov/pdf/64317main_helios.pdf`.

[25] K. Nonami, F. Kendoul, S. Suzuki, W. Wang, D. Nakazawa. *Autonomous Flying Robots: Unmanned Aerial Vehicles and Micro Aerial Vehicles* . Springer, 2010.

[26] A. Puri. A Survey of Unmanned Aerial Vehicles (UAV) for Traffic Surveillance. In *Department of Computer Science and Engineering, University of South Florida*, May 2008. [online] `http://www.csee.usf.edu/~apuri/techreport.pdf`.

[27] S. D. Hanford, L. N. Long, and J. F. Horn. A Small Semi-Autonomous Rotary-Wing Unmanned Air Vehicle (UAV). In *AIAA Infotech @ Aerospace Conference*, September 2005.

[28] W. L. Chan. Computer Aided Landing Control System Design For A Fixed Wing UAV. Master's thesis, National Cheng Kung University, 2005.

[29] J. Escareno, A. Sanchez, O. Garcia, and R. Lozano. Triple Tilting Rotor mini-UAV: Modeling and Embedded Control of the Attitude. In *American Control Conference*, June 2008.

[30] G. R. Gress. Using Dual Propellers as Gyroscopes for Tilt-Prop Hover Control. In *Biennial International Powered Lift Conference and Exhibit*, November 2002.

[31] V/STOL: The First Half-Century, Same Propulsion System for Hover and Forward Flight, July 2011. [online] `http://www.aiaa.org/tc/vstol/same.html`.

[32] Aerosonde Unmanned Aircraft System, July 2011. [online] `http://www.aerosonde.com/products/products.html`.

[33] X45B, July 2011. [online] `http://www.boeing.com/defense-space/military/x-45/`.

[34] P. McKerrow. Modelling the Draganflyer four-rotor helicopter. In *Robotics and Automation, 2004. Proceedings. ICRA '04. 2004 IEEE International Conference on*, volume 4, pages 3596–3601 Vol.4, 26-May 1, 2004.

[35] MD4-1000, July 2011. [online] `http://www.microdrones.com/produkt-md4-1000-smallbusiness-en.php`.

[36] QTW-UAS FS4, July 2011. [online] `http://www.ghcraft.com/QTW/pdf/081001_QTW_FS4e.pdf`.

[37] Eagle Eye Pocket Guide, July 2011. [online] `http://www.`

`bellhelicopter.com/en/aircraft/military/pdf/EagleEye_PG_`
`05_web.pdf`.

[38] S. Bouabdallah, A. Noth, and R. Siegwart. Pid vs lq control techniques applied to an indoor micro quadrotor. In *Intelligent Robots and Systems, 2004. (IROS 2004). Proceedings. 2004 IEEE/RSJ International Conference on*, volume 3, pages 2451 – 2456 vol.3, sept.-2 oct. 2004.

[39] P. Pounds, R. Mahony, and P. Corke. Modelling and control of a large quadrotor robot. *Control Engineering Practice*, 18(7):691 – 699, 2010. Special Issue on Aerial Robotics.

[40] A. Mokhtari and A. Benallegue. Dynamic feedback controller of euler angles and wind parameters estimation for a quadrotor unmanned aerial vehicle. In *Robotics and Automation, 2004. Proceedings. ICRA '04. 2004 IEEE International Conference on*, volume 3, pages 2359 – 2366 Vol.3, april-1 may 2004.

[41] Bauer, P. and Ritzinger, G. and Soumelidis, A. and Bokor, J. LQ Servo control design with Kalman filter for a quadrotor UAV. *Periodica Polytechnica*, 36(1-2):9–14, 2008.

[42] A. Tayebi and S. McGilvray. Attitude stabilization of a vtol quadrotor aircraft. *Control Systems Technology, IEEE Transactions on*, 14(3):562 – 571, may 2006.

[43] T. Madani and A. Benallegue. Backstepping control for a quadrotor helicopter. In *Intelligent Robots and Systems, 2006 IEEE/RSJ International Conference on*, pages 3255 –3260, oct. 2006.

[44] Abhijit Das, Frank Lewis, and Kamesh Subbarao. Backstepping approach for controlling a quadrotor using lagrange form dynamics. *J. Intell. Robotics Syst.*, 56:127–151, September 2009.

[45] S. Bouabdallah and R. Siegwart. Full control of a quadrotor. In *Intelligent Robots and Systems, 2007. IROS 2007. IEEE/RSJ International Conference on*, pages 153 –158, 29 2007-nov. 2 2007.

[46] Ashfaq Ahmad Mian and Wang Daobo. Modeling and backstepping-based nonlinear control strategy for a 6 dof quadrotor helicopter. *Chinese Journal of Aeronautics*, 21(3):261 – 268, 2008.

[47] T. Madani and A. Benallegue. Backstepping control with exact 2-sliding mode estimation for a quadrotor unmanned aerial vehicle. In *Intelligent Robots and Systems, 2007. IROS 2007. IEEE/RSJ International Conference on*, pages 141 –146, 29 2007-nov. 2 2007.

[48] T. Madani and A. Benallegue. Sliding mode observer and backstepping control for a quadrotor unmanned aerial vehicles. In *American Control Conference, 2007. ACC '07*, pages 5887 –5892, july 2007.

[49] L. Besnard, Y.B. Shtessel, and B. Landrum. Control of a quadrotor vehicle using sliding mode disturbance observer. In *American Control Conference, 2007. ACC '07*, pages 5230 –5235, july 2007.

[50] Daewon Lee, H. Jin Kim, and Shankar Sastry. Feedback linearization vs. adaptive sliding mode control for a quadrotor helicopter. *International Journal of Control, Automation and Systems*, 7:419–428, 2009. 10.1007/s12555-009-0311-8.

[51] Rong Xu and Umit Ozguner. Sliding mode control of a class of under-actuated systems. *Automatica*, 44(1):233–241, 2008.

[52] A. Mokhtari, A. Benallegue, and Y. Orlov. Exact linearization and sliding mode observer for a quadrotor unmanned aerial vehicle. *Int. J. Robot. Autom.*, 21:39–49, January 2006.

[53] A. Benallegue, A. Mokhtari, and L. Fridman. High-order sliding-mode observer for a quadrotor uav. *International Journal of Robust and Non-linear Control*, 18(4-5):427–440, 2008.

[54] Zhou Fang, Zhang Zhi, Liang Jun, and Wang Jian. Feedback lineariza-tion and continuous sliding mode control for a quadrotor uav. In *Control Conference, 2008. CCC 2008. 27th Chinese*, pages 349 –353, july 2008.

[55] H. Voos. Nonlinear control of a quadrotor micro-uav using feedback-linearization. In *Mechatronics, 2009. ICM 2009. IEEE International Conference on*, pages 1 –6, april 2009.

[56] S.A. Al-Hiddabi. Quadrotor control using feedback linearization with dynamic extension. In *Mechatronics and its Applications, 2009. ISMA '09. 6th International Symposium on*, pages 1 –3, march 2009.

[57] T. Dierks and S. Jagannathan. Neural network output feedback control of a quadrotor uav. In *Decision and Control, 2008. CDC 2008. 47th IEEE Conference on*, pages 3633 –3639, dec. 2008.

[58] T. Dierks and S. Jagannathan. Output feedback control of a quadrotor uav using neural networks. *Neural Networks, IEEE Transactions on*, 21(1):50 –66, jan. 2010.

[59] C. Nicol, C.J.B. Macnab, and A. Ramirez-Serrano. Robust neural network control of a quadrotor helicopter. In *Electrical and Computer Engineering, 2008. CCECE 2008. Canadian Conference on*, volume 1, pages 001233 –001238, may 2008.

[60] H. Voos. Nonlinear and neural network-based control of a small four-rotor aerial robot. In *Advanced intelligent mechatronics, 2007 IEEE/ASME international conference on*, pages 1 –6, sept. 2007.

[61] Guilherme V. Raffo, Manuel G. Ortega, and Francisco R. Rubio. An integral predictive/nonlinear h_∞; control structure for a quadrotor helicopter. *Automatica*, 46:29–39, January 2010.

[62] H. Chen and M. Huzmezan. A combined mbpc / 2 dof h_∞ controller for a quad rotor uav. In *2003 AIAA Guidance, Navigation, and Control Conference*, pages 26 –32, sept. 2003.

[63] A. Mokhtari, A. Benallegue, and B. Daachi. Robust feedback linearization and gh infin; controller for a quadrotor unmanned aerial vehicle. In *Intelligent Robots and Systems, 2005. (IROS 2005). 2005 IEEE/RSJ International Conference on*, pages 1198 – 1203, aug. 2005.

[64] K. T. Oner. Modeling and Control of a New Unmanned Aerial Vehicle (SUAVI) with Tilt-Wing Mechanism. Master's thesis, Sabanci University, 2009.

[65] E. Cetinsoy. Design, Construction and Flight Control of a Quad Tilt-Wing Unmanned Aerial Vehicle. Master's thesis, Sabanci University, 2010.

[66] C. Hancer. GPS Based Position Control and Waypoint Navigation of a Quad Tilt-Wing UAV. Master's thesis, Sabanci University, 2010.

[67] E. Sirimoglu. Prototyping and Hierarchical Control of a Quad Tilt-Wing UAV. Master's thesis, Sabanci University, 2010.

[68] F. Kendoul, I. Fantoni, and R. Lozano. Asymptotic stability of hierarchical inner-outer loop-based flight controllers. In *in Proceedings of the 17th IFAC World Congress, 2008.*, pages 1741 – 1746, July 2008.

[69] V. Utkin and J. Guldner and J. Shi. *Sliding Mode Control in Electromechanical Systems.* CRC Press, 1999.

[70] Steven L. Waslander and Carlos Wang. Wind disturbance estimation and rejection for quadrotor position control. *In AIAA Infotech@Aerospace Conference and AIAA Unmanned...Unlimited Conference*, April 2009.